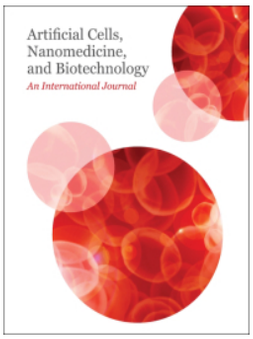

Taylor & Francis
Taylor & Francis Group

Artificial Cells, Nanomedicine, and Biotechnology
An International Journal

ISSN: (Print) (Online) Journal homepage: www.tandfonline.com/journals/ianb20

Computational metal-flavonoids complexes presentation of greenly synthesized silver nanoparticles combined flavonoids from *Lens culinaris L.* as anticancer agents using BcL-2 and IspC proteins

Heba W. Alhamdi, Fatma Alzahraa Mokhtar, Fouad Lamghari Ridouane, Ali A. Shati, Serag Eldin I. Elbehairi, Lamiaa I. Fahmy, Mohammad Y. Alfaifi, Nada K. Sedky & Heba A. Fahmy

To cite this article: Heba W. Alhamdi, Fatma Alzahraa Mokhtar, Fouad Lamghari Ridouane, Ali A. Shati, Serag Eldin I. Elbehairi, Lamiaa I. Fahmy, Mohammad Y. Alfaifi, Nada K. Sedky & Heba A. Fahmy (2024) Computational metal-flavonoids complexes presentation of greenly synthesized silver nanoparticles combined flavonoids from *Lens culinaris L.* as anticancer agents using BcL-2 and IspC proteins, Artificial Cells, Nanomedicine, and Biotechnology, 52:1, 529-550, DOI: 10.1080/21691401.2024.2420414

To link to this article: https://doi.org/10.1080/21691401.2024.2420414

ARTIFICIAL CELLS, NANOMEDICINE, AND BIOTECHNOLOGY
2024, VOL. 52, NO. 1, 529–550
https://doi.org/10.1080/21691401.2024.2420414

Computational metal-flavonoids complexes presentation of greenly synthesized silver nanoparticles combined flavonoids from *Lens culinaris L.* as anticancer agents using BcL-2 and IspC proteins

Heba W. Alhamdi[a*], Fatma Alzahraa Mokhtar[b,c*], Fouad Lamghari Ridouane[b], Ali A. Shati[d,e], Serag Eldin I. Elbehairi[d,e], Lamiaa I. Fahmy[f], Mohammad Y. Alfaifi[d,e], Nada K. Sedky[g] and Heba A. Fahmy[h]

[a]Department of Biology, College of Sciences, King Khalid University, Abha, Saudi Arabia; [b]Fujairah Research Centre, Sakamkam Road, Fujairah, United Arab Emirates; [c]Department of Pharmacognosy, Faculty of Pharmacy El Saleheya El Gadida University, El Saleheya El Gadida, Sharkia, Egypt; [d]Biology Department, Faculty of Science, King Khalid University, Abha, Saudi Arabia; [e]Tissue Culture and Cancer Biology Research Laboratory, King Khalid University, Abha, Saudi Arabia; [f]Department of Microbiology and Immunology, Faculty of Pharmacy, October University for Modern Sciences and Arts (MSA), Giza, Egypt; [g]Department of Biochemistry, School of Life and Medical Sciences, University of Hertfordshire hosted by Global Academic Foundation, Cairo, Egypt; [h]Pharmacognosy Department, Faculty of Pharmacy, Modern University for Technology & Information, Cairo, Egypt

ABSTRACT

Lens culinaris L., has been widely recognized for its medical applications. LC-ESI-TOF-MS identified 22 secondary metabolites including phenolics, flavonoids, and anthocyanidin glycosides among its total extract (LCTE). The study aimed to apply LCTE as a biogenic material for reducing and capping the silver nanoparticles (LC-AgNPs). The ynthesized LC-AgNPs were characterized using different techniques. The UV absorption was observed at λ_{max} 379 nm. LC-AgNPs were spherical, with 19.22 nm average size. The face cubic centre nature was demonstrated by HR-TEM and XRD. The LC-AgNPs were then evaluated for their anticancer and antimicrobial potentials. LC-AgNPs showed an extremely potent cytotoxic activity against MCF-7, HCT-116 and HepG2 cell lines (IC_{50}= 0.37, 0.35 and 0.1 µg/mL, respectively). LC-AgNPs induced significant apoptotic effects in the three examined cancer cell lines. LC-AgNPs resulted in sequestration of cells in G1 phase of the cell cycle in both MCF-7 and HCT-116 cells, meanwhile it trapped cells at the G2 phase in HepG2 cells. Moreover, the antimicrobial activity of LC-AgNPs was highly confirmed against *Klebsiella pneumoniae* and *Acinetobacter baumannii*. Molecular docking study designated Kaempferol-3-O-robinoside-7-O-rhamnoside and Quercetin-3-D-xyloside as the topmost LCTE active constituents that caused inhibition of both Bcl-2 and IspC cancer targets in combination with the produced silver nanoparticles.

ARTICLE HISTORY
Received 18 July 2024
Revised 29 August 2024
Accepted 1 October 2024

KEYWORDS
Lens culinaris; silver nanoparticles; green synthesis; cytotoxicity; antimicrobial

Introduction

Nanotechnology has shown a distinguished series of successes in biotechnology, medicine, energy conservation, and water treatment. Currently, the interest in metal nanoparticles is growing owing to their recoverability, ease in production, diagnostic and treatment applications [1–3]. Silver and its oxides are among the different metal nanoparticles (NPs) that have gained special attention because of their remarkable physiochemical properties and minimal toxicity [4]. In addition, silver nanoparticles such as Ag-doped CuO nanoparticles were reported to possess biosensing properties, which render their biological traceability an easy process [5]. Generally, amines and alcohols are used as reducing or capping agents to produce AgNPs colloidal solutions from Ag [6]. However, the majority of chemicals used in such processes are hazardous to people and the environment, which in turn necessitates the use of a "green synthesis" method. Green nanotechnology utilizes natural green sources as plants, fungi, and bacteria instead of hazardous chemicals in the production of nanomaterials [7–11]. The biogenic fabrication of silver nanoparticles from plant extracts was found to magnify the possible pharmacological and pharmaceutical applications especially anticancer and antimicrobial activities [12,13]. For instance, green synthesized silver-iron oxide bimetallic nanoparticles displayed potent antioxidant and catalytic activities [14]. A recent study by Gupta and colleagues also reported significant antioxidant, catalytic, and anticancerous activities for the Ag-Fe-Ni trimetallic nanoparticles made from orange peel [15].

Lens culinaris L., commonly known as lentil (Family *Fabaceae*) is a very important traditional dietary element [16].

CONTACT Nada K. Sedky n.sedky@gaf.edu.eg; ns20acf@herts.ac.uk Department of Biochemistry, School of Life and Medical Sciences, University of Hertfordshire hosted by Global Academic Foundation, Cairo, Egypt; Fatma Alzahraa Mokhtar drfatmaalzahraa1950@gmail.com Fujairah Research Centre, Sakamkam Road, Fujairah, United Arab Emirates

Supplemental data for this article can be accessed online at https://doi.org/10.1080/21691401.2024.2420414.

*Both authors have equally contributed.

Lentils are regarded as an ancient legume because of their prehistoric origins, but in the present era, they are grown in more than 35 countries on five continents. The Food and Agriculture Organization (FAO) mentioned that the production of lentils increased significantly between 2001 and 2014, whereby reaching 5 million tonnes annually. Lentils are generally rich in proteins, nutrients and minerals [17]. Moreover, Lentils contain carbohydrates [18], fatty acids [19], magnesium (Mg), phosphorus (P), calcium (Ca), sulphur (S), selenium (Se) [20] and vital vitamins like niacin, B1, B2, E and K [17]. Lentils are crucial to the food industry process, merely, the production of baked goods, flour mixtures, gluten-free, snack, dairy products, and meat extenders [21]. It is worth mentioning that lentils possess high concentrations of bioactive phytochemicals, such as tannins and polyphenols. Red lentils have a high content of catechin, quercetin diglycoside, *p*-hydroxybenzoic, and procyanidin [22,23]. Interestingly, green or red whole lentils surpassed the pale ones in regard to their phenolic composition [24]. Lentil seeds comprise a high content of phytosterols (*β*-sitosterol) [25], saponins (their content depends on germination conditions) [26], dietary fibres (protect against constipation) [27], lectins and phytic acid [28].

Lentils have been traditionally used to treat a variety of ailments including diabetes [29], skin infections [30], and burns [31]. A vast amount of research work supports its beneficial role as a hypocholesterolemic, hypoglycaemic, antihypertensive, antibacterial, anti-oxidant and anticarcinogenic agent [32]. Furthermore, numerous studies showed a negative correlation between lentils consumption and the risk of cancer development in certain tissues as breast [33], prostate [34], and colon [35]. This could be attributed to its constituents including polyphenols [36], lectins, bioactive peptides [37], folic acid [38], saponins [26], and selenium [39], as well as its low glycemic index [40].

This research contributes to the growing field of green nanotechnology by exploring the potential of *Lens culinaris L. (Lentil)* as a sustainable and biocompatible source for nanoparticle synthesis. While previous research demonstrated the anticancer and antibacterial potential of *Lens culinaris* [41,42], the particular assessment of the nanoparticles produced using *Lens culinaris* seeds [43] has not been investigated. This study is the first to formulate silver nanoparticles from *Lens culinaris* seeds and discuss their therapeutic potential. This unexplored area presents a significant opportunity to develop novel effective antibacterial and anticancer agents. By biological and cellular investigations of the underlying mechanism of action, the study establishes a direct link between the plant's chemical composition and its observed therapeutic benefits, paving the way for future development and optimization. The virtual chemical study is the premier to illustrate the synergistic potential of the silver nanoparticles and the extracts' flavonoids when applied to the target proteins (Bcl-2 and IspC). This entails the role of the natural LCTE extract as a functioning element to potentiate the anticancer activity of the silver nanoparticles. Concisely, the current work presents a notable link between *Lens Culinaris* chemical constituents, silver nanoparticles, and the observed biological activities.

Materials and methods

Plant material

Lens culinaris L. seeds were purchased from the Egyptian local market. Authentication was done by Dr. Esra Amaar, a plant scientist at Tanta University. The voucher specimen (PG-A-LC-F-107) was kept at Tanta University's Herbarium. The seeds were grinded to fine powder before extraction.

Preparation of Lens extract

Powdered seeds (100 g) were macerated in 70% ethanol. They were put on a shaker for 30 min at 50 °C and the process was repeated 3 times. After filteration, the extract was centrifuged, and the supernatant was concentrated under vacuum at 45 °C. The yielded concentrated mass was further purified with absolute ethanol. The supernatant was filtered and evaporated at room temperature to form a dry residue.

LC-ESI-TOF-MS analysis for metabolite profiling

Sample preparation

LCTE dry residue (50 mg) was dissolved in 1 ml reconstitution solvent (deionized water, methanol, and acetonitrile; 50:25:25). Then, it was vortexed, ultrasonicated, and centrifuged. Directly afterwards, it was diluted and 10 µL (2.5 µg/µL) was injected.

Instruments and acquisition method

LC-ESI-TOF-MS (liquid chromatography–electrospray ionization–tandem mass spectrometry) assessment conditions adopted were previously described in [44] at the Hospital of Children's Cancer (57357) Proteomics and Metabolomics Research Unit. For chromatographic separation, a column with the specifications of X select HSS T3 (Waters Corporation, Milford, MA, USA) was used. Additionally, a precolumn with dimensions of 0.5 m × 3.0 mm (Phenomenex, Torrance, CA, USA) was utilized. Both the column and precolumn were managed at a 40 °C temperature. Sodium hydroxide was used to adjust the pH of mobile phase (A) to a value of 8. A 1% methanol solution containing 5 mM ammonium formate was used as the mobile phase. The binary gradient elution system was kept operating at a flow rate of 300 L per minute. The study used the information-dependent acquisition (IDA) approach to carry out the experiment. The Analyst-TF 1.7.1 software was used to prepare the data collection batches for MS and MS/MS. The collection of full-scan MS and MS/MS data was made easier by the use of IDA. The survey spectra obtained were of good resolution and included the mass-to-energy range of 50–1000 *m/z*.

Data processing for LC-MS

MS-DIAL 4.6 software [45] was utilized for the comprehensive analysis of the sample, using ReSpect negative with 1573 records as a reference database. Search parameters were adjusted as published before by Elbalawi et al. [46]. The output of MS-DIAL was run on PeakView with the MasterView

package for peaks (features) confirmation from TIC (Total Ion Chromatogram).

Biogenic formation of AgNPs

A millimolar of silver nitrate ($AgNO_3$) aqueous solution was produced. The mixture was kept in a cold, dark place. LCTE (10 ml) was added to the prepared solution of $AgNO_3$ (1 mM; 90 ml). It was left overnight in a dimly lit space. These conditions allow the reduction of Ag ions. The emergence of a yellowish-brown hue indicated the AgNPs' development. The prepared solutions were submitted to TEM and UV testing instantly. To get pure AgNPs, centrifugation at 4000 rpm for 30 min was the first step. The second step was triplicate wash steps with distilled water followed by filtration. The third step was triplicate wash in absolute ethanol. Fourier-Transform Infra-red (FTIR), High-Resolution Transmission Electron Microscope (HR-TEM), X-ray Diffraction (XRD), Zeta Potential, and Scanning Electron Microscope (SEM) were deployed to examine the generated LC-AgNPs in detail.

LC-AgNPs characterization

UV-Vis spectroscopy

A UV-Vis spectrophotometer (Shimadzu, Kyoto, Japan) was used to monitor the UV-Vis spectroscopy of the LCTE and LC-AgNPs. Following the dilution of the samples with distilled water, the absorbance was determined.

FTIR

An FTIR spectrometer (Jasco, Tokyo, Japan) was used to characterize LCTE and LC-AgNPs functional groups in the 4000–400 cm − 1 range.

HR-TEM

LC-AgNPs morphology (shape and size) besides SAED were detected by (JEOL-JEM 2100, Kyoto, Japan). For HR-TEM examinations, 3 ml of the sample were deposited on the copper grid and allowed to dry at room temperature for 15 min as described before [12].

SEM

As previously described [47], the biogenic AgNPs' morphology was examined using the SEM (TM1000, Hitachi, Chiyoda, Japan).

Zeta potential

LC-AgNPs were subjected to examination of their charge and particle size using a zeta sizer nano ZN (Malvern Panalytical Ltd., England, UK) [48].

XRD

The XRD analysis was used to characterize metal nanoparticles as a surface chemical analysis method. An XPERT-PRO-PANalytical Powder Diffractometer (PAN-analytical B.V., Almelo, The Netherlands) was used for X-ray analysis. The monochromatic Cu-K radiation source (=1.5406) was operated at room temperature at 45 kV and 30 mA. The intensity of silver nanopowder was measured at a range of 4.01°–79.99° [49].

Cytotoxicity

Cell culture

Human breast cancer (MCF-7), colorectal carcinoma (HCT-116), and hepatoma (HepG2) cell lines were acquired from ATCC (American type of culture collection). The culture medium used to grow the cells was RPMI-1640, which also contained penicillin (100 units/mL) and heat-inactivated foetal bovine serum (10% *v/v*). The culture plates were kept at 37 °C in a humidified incubator with 5% (*v/v*) CO_2.

Cytotoxicity assay

Sulforhodamine B (SRB) assay was employed to determine the cytotoxicity of LCTE and LC-AgNPs against MCF-7, HCT-116, and HepG2 cancer cells. The 96-well plates were used for cell culture. The plates containing the cultured cells were left in the incubator for one day. Then, different concentrations of LCTE and LC-AgNPs (0.01, 0.1, 1, 10, 100 and 1000 µg/mL) were added to the cells. Untreated cells were utilized as a control group. The cells were incubated with the applied treatments at 37 °C for three days. Thereupon, the cells were treated with TCA (10% *w/v*) and placed for 1 h in the fridge for fixation. The cells were washed several times after fixation. Directly afterwards, 0.4% (*w/v*) SRB solution was applied to the cells and left for 10 min in a dim chamber. Glacial acetic acid (1% *v/v*) was used to wash the cells before leaving them to dry for the entire night. The next morning, Tris-HCl was added to detach the SRB-stained cells, and absorbance was measured at 540 nm (using spectrophotometer (Shimadzu, Kyoto, Japan)) utilizing a microplate reader. Lastly, Sigma Plot 12.0 software was used to compute the IC_{50} of the test compounds.

Apoptosis analysis

The apoptosis assay was carried out using the Annexin V-FITC/PI Apoptosis Detection Kit from Cell Signalling Technology (Massachusetts, USA). The assay was performed as prescribed in Kit' guidelines and following a previously published study [50]. Cells were treated with the pre-estimated IC_{50} values of LCTE and LC-AgNPs for 48 h. This was followed by trypsinization of cells and washing with PBS for 2 consecutive times. Cells were then suspended in Annexin V-FITC (5 µL) and PI (staining solution; 5 µL). Thereafter, an estimate of 0.5 ml binding buffer was applied to the cell suspension with a good mixing. The cells were left at 25 °C in a dark room for only 15 min. At the end, cells were injected into Cytek® Northern Lights 2000 spectral flow cytometer (Cytek Biosciences, USA) and quadrant analysis was performed using the built-in software (SpectroFlo™ Software version 2.2.0.3).

Cell cycle analysis

For 48 h, cells were exposed to the pre-calculated IC_{50} values of LCTE and LC-AgNPs. This was followed by trypsinization of cells and washing them with PBS. Directly afterwards, a

fixation step was performed with ice-cold 60% ethanol and one more wash step with ice-cold PBS. A mixture of 500 µL of propidium iodide (PI) and RNase staining buffer (Cell Signalling Technology, Massachusetts, USA) were then applied to the cells. The cells were kept for 15 min away from light. Finally, cells were injected into a Cytek® Northern Lights 2000 spectral flow cytometer (Cytek Biosciences). About 10,000 cells were aquired for each sample. The SpectroFloTM Software version 2.2.0.3 was deployed for calculating the percentage of cells at each phase of the cell cycle. The whole method was adopted from colleagues' work [50].

Antibacterial activity

Determination of antibacterial activity

The antibacterial effects of LCTE and LC-AgNPs were assayed using the Agar well diffusion technique. The bacteria were subcultured on LB medium and incubated for 24 h at 37 °C. Bacterial cultures were spread on the agar plate. Two types of Gram-negative bacteria were used such as the strong biofilm-forming isolate of *Klebsiella pneumoniae* (K21) and the extensive drug-resistant isolate *(*XDR) of *Acinetobacter baumannii* (M18) [51]. LCTE and LC-AgNPs were tested against these bacteria. The bacteria were incubated for 24 h at 37 °C. To evaluate the antibacterial activity of LCTE and LC-AgNPs, the inhibition zone was measured compared to the control groups. The results were interpreted according to CLSI [52].

Molecular docking

In vitro, study has revealed that both LCTE and its AgNPs possess a significant cytotoxic effect against MCF-7, HCT-116, and HepG2 cell lines. Their anticancer activity is mainly exerted by inducing the apoptotic pathways via down-regulation of Bcl-2. Accordingly, we investigate how AgNPs and LCTE can bind to the active pocket of Bcl-2. Bcl-2 inhibitors are reported to inhibit the antiapoptotic Bcl-2 protein via binding to the binding groove [53]. 17 major classes of detected compounds in *Lens culinaris* L (Figure 1) in addition to AgNPs were docked against Bcl-2 x-ray crystal structure (PDB ID. 2W3L). The Crystal Structure of Chimaeric Bcl2-xL in complex with phenyl tetrahydroisoquinoline amide was downloaded from Protein Data Bank (PDB ID: 2W3L; http://www.rcsb.org/structure/2W3L).

In *Acinetobacter baumannii* and *Klebsiella pneumonia*, Deoxy-d-Xylulose 5-Phosphate Reductoisomerase (IspC) was chosen as a potential therapeutic target [54]. IspC in complex with FR900098, NADPH, and a magnesium ion was downloaded from PDB with PDB ID. 7S04 (http://www.rcsb.org/structure/7S04).

Water molecules in the two crystal structures were deleted using AutoDock tools and polar hydrogen atoms were added. Partial charges of Marsili-Gasteiger are assigned using a two-step algorithm. The receptor crystal structures were subjected to energy minimization using the AutoDockTools (ADT, v1.5.6), and the prepare_receptor4.py command to calculate the partial atomic charge using the Kollman-united charge method [55].

LCTE 17 major molecules were prepared via AutoDockTools (ADT, v1.5.6) by manipulating the prepare_ligand4.py command and saved in PDBQT format. The grid box dimension was optimized surrounding the co-crystallized ligands in both x-ray crystals. The structure of AgNP was drawn using ChemSketch and its geometry was optimized by Autodock

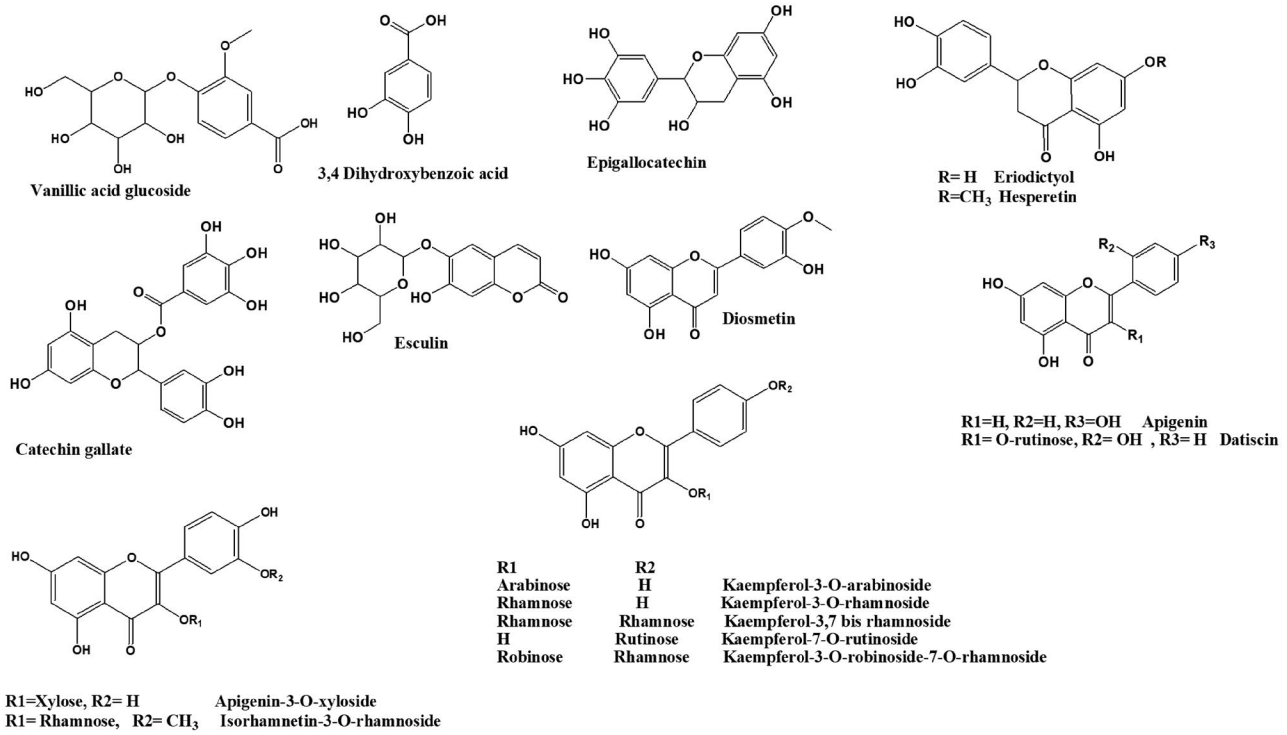

Figure 1. Major classes of detected compounds in *Lens culinaris L.*

Table 1. Secondary metabolites identified in *Lens culinaris* via LC–ESI-TOF–MS.

	Title	Class	RT (min.)	$[M–H]^-$	MS/MS	Formula	Ref.
1	Neohesperidin dihydrochalcone	Flavanone derivative (chalconoids)	1.37	611.04	465.1, 303.1	$C_{28}H_{36}O_{15}$	[58]
2	Vanillic acid glucoside	Phenolic acid (hydroxybenzoic acids)	4.12	329.31	167.3, 152.7	$C_{14}H_{18}O_9$	[59]
3	3,4-Dihydroxybenzoic acid	Phenolic acid (hydroxybenzoic acids)	4.88	153.11	107.4	$C_7H_6O_4$	[60]
4	Kaempferol-3-*O*-robinoside-7-*O*-rhamnoside	O-flavonoid glycoside	5.03	739.42	593.0, 481.2	$C_{33}H_{40}O_{19}$	[61]
5	Kaempferol 7-*O*-rutinoside	O-flavonoid glycoside	6.15	593.27	431.3, 285.0	$C_{27}H_{30}O_{15}$	[60]
6	Linarin	Flavone glycoside	6.53	591.05	283.3	$C_{28}H_{32}O_{14}$	[62]
7	Kaempferol-3,7-*O*-bis-rhamnoside	O-flavonoid glycoside	6.83	577.13	431.1, 285.0	$C_{27}H_{30}O_{14}$	[63]
8	Quercitrin	Flavonol	7.14	447.22	301.2	$C_{21}H_{20}O_{11}$	[64]
9	Kaempferol-3-*O*-rhamnoside	O-flavonoid glycoside	7.948	431.03	284.8	$C_{21}H_{20}O_{10}$	[65]
10	Kaempferol-3-*O*-arabinoside	O-flavonoid glycoside	8.36	417.25	285.1	$C_{20}H_{18}O_{10}$	[66]
11	Catechin gallate	Falvan-3-ols	8.96	441.44	289.3, 220.8	$C_{22}H_{18}O_{10}$	[67]
12	Epigallocatechin	Falvan-3-ols	9.31	305.06	275.2	$C_{15}H_{14}O_7$	[68]
13	Eriodictyol	Flavanones	9.75	287.17	255.4, 151.0	$C_{15}H_{12}O_6$	[69]
14	Delphinidin 3,5-diglucoside	Anthocyanidin glycoside	10.44	627.33	302.7	$C_{27}H_{31}O_{17}$	[70]
15	Cyanidin-3-*O*-(2″-*O*-glucopyranosyl-glucopyranoside)	Anthocyanidin glycoside	10.77	611.34	287.3	$C_{27}H_{31}O_{16}$	[71]
16	Datiscin	Flavonol glycoside	11.04	593.29	285.1, 212.6	$C_{27}H_{30}O_{15}$	[72]
17	Isorhamnetin rhamnoside	Flavonol glycoside	11.50	461.03	315.1, 300.5	$C_{22}H_{22}O_{11}$	[73]
18	Diosmetin	Flavone	12.92	299.40	285.3	$C_{16}H_{12}O_6$	[71]
19	Quercetin-3-xyloside	Flavonol glycoside	14.11	433.12	300.7, 179.2	$C_{20}H_{18}O_{11}$	[63,73]
20	Hesperetin	Flavanones	15.75	301.36	174.8	$C_{16}H_{14}O_6$	[67]
21	Esculin	Coumarin glucoside	16.34	339.09	177.3	$C_{15}H_{16}O_9$	[74]
22	Apigenin	Flavone	18.53	269.03	225.4	$C_{15}H_{10}O_5$	[75]

4.2. For NP docking it was allowed to be docked in all the protein pockets to find a suitable allosteric site for binding. The docking parameters were set to 2.500.00 energy evaluation, 100 runs number, and 150 for size of population based on Lamarckian genetic algorithm [56]. Ten binding modes were produced for the ligand with a maximum of 3 kcal/mol energy difference between each mode and the best conformations, showing lowest binding free energy were retrieved. BIOVA Discovery Studio visualizer 2021 was used to generate 2D interaction figures and PyMOL(TM) 2.5.2 was used for generating 3D interaction figures [57].

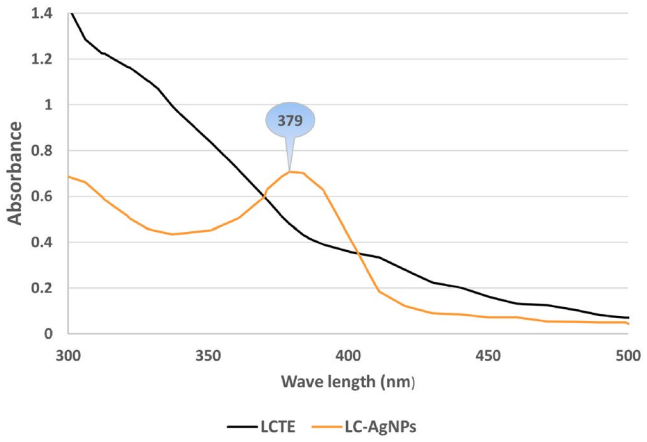

Figure 2. UV spectrum of LC-AgNPs compared to LCTE.

Results and discussion

Chromatographic analysis of LCTE by LC-ESI-MS/MS

The metabolic profiling of *Lens culinaris* using negative-mode ESI-TOF-MS identified 22 secondary metabolites, albeit tentatively. The metabolites that were found were categorized as simple phenolics, phenolic acid derivatives, flavonoids, flavonoid glycosides, and anthocyanidin glycosides. Their retention time, molecular ion peaks, fragmentation peaks, and molecular formulae are displayed in Table 1. The TIC of *Lens culinaris* is presented in Figure S1. The structures of the identified metabolites are provided in Figure 1.

Identification of simple phenolics and phenolic acid derivatives

The phenolic acids identified in *Lens* seed extract were mainly hydroxybenzoic and represented by vanillic acid glucoside and 3,4-dihydroxybenzoic acid. Vanillic acid glucoside (2) with molecular ion peak $[M–H]^-$ at *m/z* 329 and characteristic fragment ions 167 corresponding to the deprotonated vanillic acid [59]. The 3,4-dihydroxybenzoic acid (3) was identified with $[M–H]^-$ at *m/z* 153 and it gave a daughter ion peak at *m/z* 107 due to the loss of CO_2 [60]. Furthermore, a coumarin glucoside, esculin (21), was detected with $[M–H]^-$ at *m/z* 339 and a daughter ion peak at *m/z* 177 owing to the loss of glucose moiety.

Flavonoid glycosides

Using LC-MS/MS, flavonoids, and flavonoids' mono- and diglycosides were identified in the *Lens* seed. Several flavonols were identified as derivatives of kaempferol, quercetin, isorhamnetin and datiscetin. Two quercetin glycosides were detected *viz.* quercitrin (Peak 8) and quercetin-3-D-xyloside (19) and characterised by the presence of base peak of $[M–H]^-$ at *m/z* 301. Quercetin-3-xyloside gave $[M–H]^-$ at *m/z* 433 and $[(M–H)-132]^-$ at *m/z* 301. Kaempferol glycosides showed a distinctive base peak of $[M–H]^-$ at *m/z* 285 and they included kaempferol-3-*O*-robinoside-7-*O*-rhamnoside (4), kaempferol-7-*O*-rutinoside (5), kaempferol-3,7-*O*-bis-rhamnoside (7),

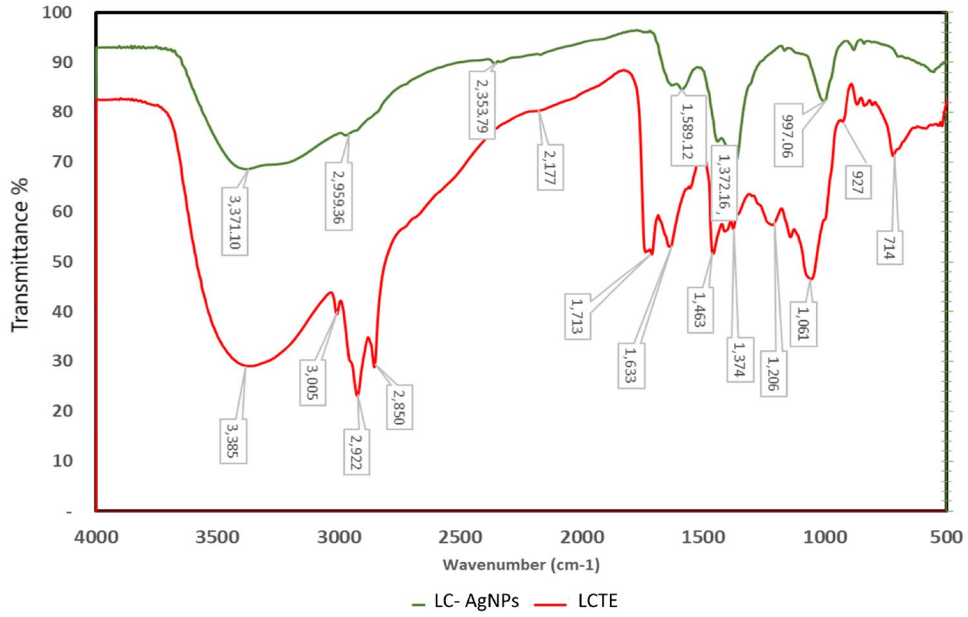

Figure 3. FTIR spectrum of LC-AgNPs compared to LCTE.

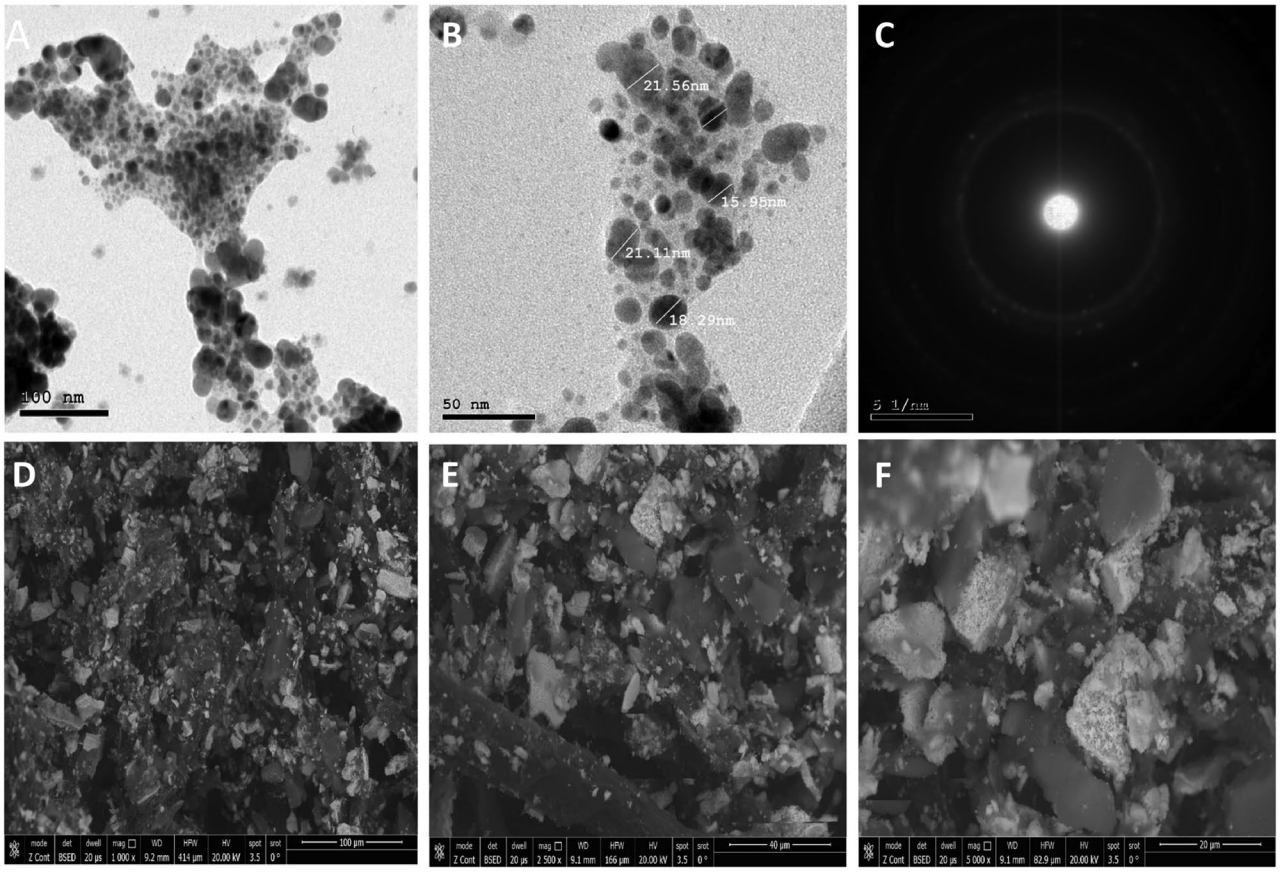

Figure 4. HR-TEM and SEM micrographs of LC-AgNPs; (A) HR-TEM at 100 nm, (B) HR-TEM at 50 nm, (C) SAED of LC-AgNPs, (D) SEM at 100 µm, (E) SEM at 40 µm, (F) SEM at 20 µm.

kaempferol-3-*O*-rhamnoside (9), and kaempferol-3-*O*-arabinoside (10). Kaempferol-3-*O*-robinoside-7-*O*-rhamnoside, kaempferol-3,7-*O*-bis-rhamnoside and kaempferol-3-*O*-rhamnoside with $[M–H]^-$ at *m/z* 739, 577, and 431, showed daughter ion peaks resulting from the loss of rhamnosyl unit $[(M–H)-146]^-$ at *m/z* 593, 431 and 285, respectively. While kaempferol-7-*O*-rutinoside with a molecular ion peak of $[M–H]^-$ at *m/z* 593 produced fragment ion peaks at 431 and 285 due to the loss of a glucosyl (–162 amu) and rutinoside (–308 amu) moieties. Isorhamnetin rhamnoside was identified at peak 17 with a

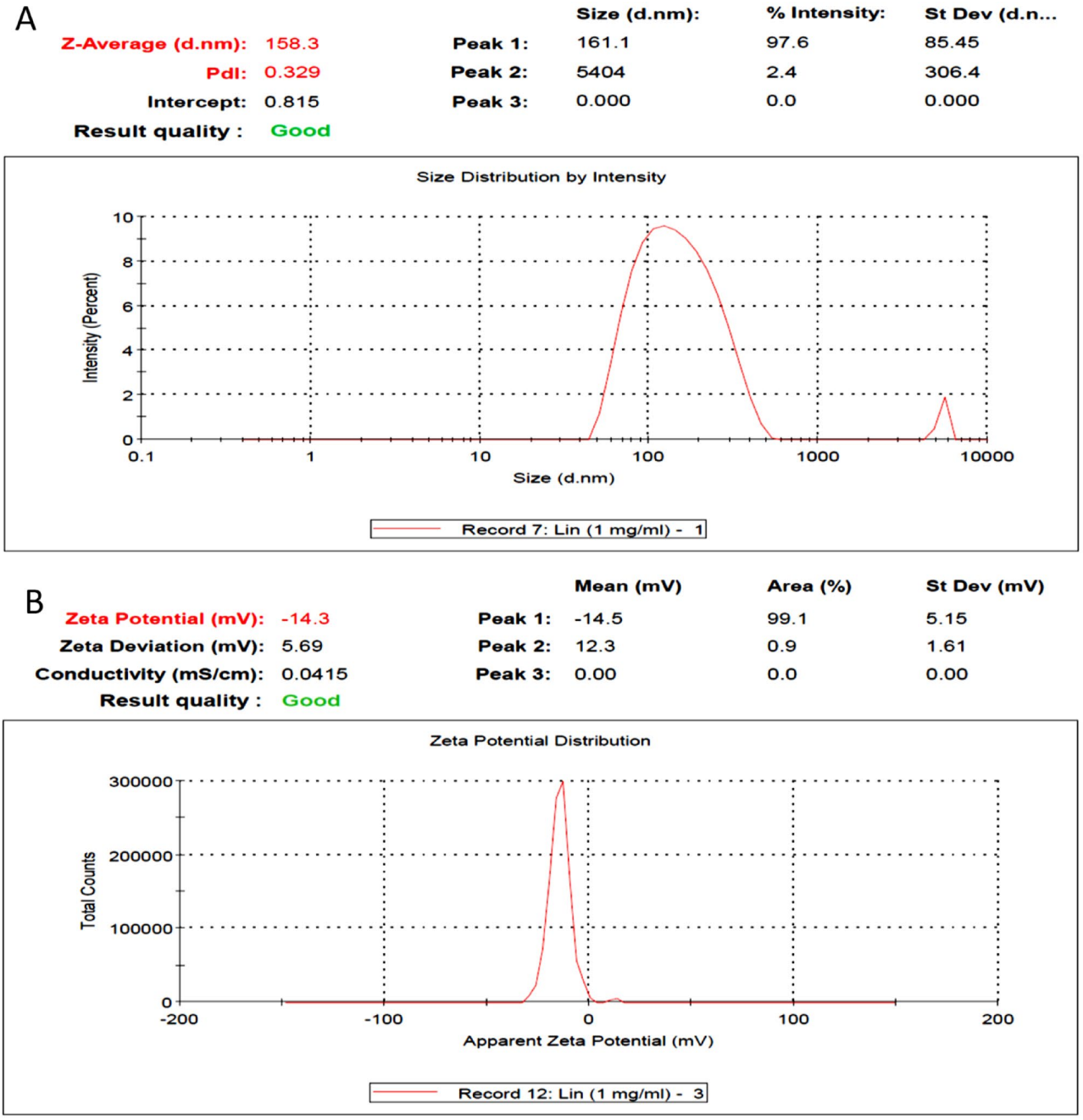

Figure 5. Zeta potential charge (A) and size (B) of the biogenic LC-AgNPs.

molecular ion peak of $[M–H]^-$ at *m/z* 461 and its base peak ions of $[M–H]^-$ at *m/z* 315, whereas datiscin (16), the datiscetin-3-rutinose, was assigned having a molecular ion peak of $[M–H]^-$ at *m/z* 593 and the characteristic fragment ion peak at 285. On the other hand, a flavone glycoside was detected as linarin (6) with a molecular ion peak of $[M–H]^-$ at *m/z* 591 and a base peak of $[M–H]^-$ at *m/z* 283.

Flavonoid aglycones were detected in *Lens* seed as eriodictyol (13), diosmetin (18), hesperetin (20), and apigenin (22) with deprotonated molecular ion peaks at *m/z* 287, 299, 301, and 269, respectively. Another flavanone derivative was assigned as neohesperidin dihydrochalcone (1) showing a molecular ion peak of $[M–H]^-$ at *m/z* 611. Neohesperidin dihydrochalcone, an artificial sweetener derived from citrus fruits, had been synthesised from neohesperidin [76] and it was previously isolated from *Oxytropis myriophylla* (family *Leguminosae)* whole plant extract [77]. Two falvan-3-ols were assigned in *Lens* seed as catechin gallate (11), epigallocatechin (12) with molecular ion peaks of $[M–H]^-$ at *m/z* 441 and 305, respectively.

Anthocyanidin glycosides

Anthocyanidin glycosides were detected in *Lens culinaris* rationalising for its characteristic yellow colour. Anthocyanins detected in *Lens* seed were represented by delphinidin and cyanidin glycosides. Delphinidin 3,5-diglucoside (14) and cyanidin-3-*O*-(2″-*O*-glucopyranosyl- glucopyranoside) (15) were assigned and their molecular ion peaks $[M-H]^-$ appeared

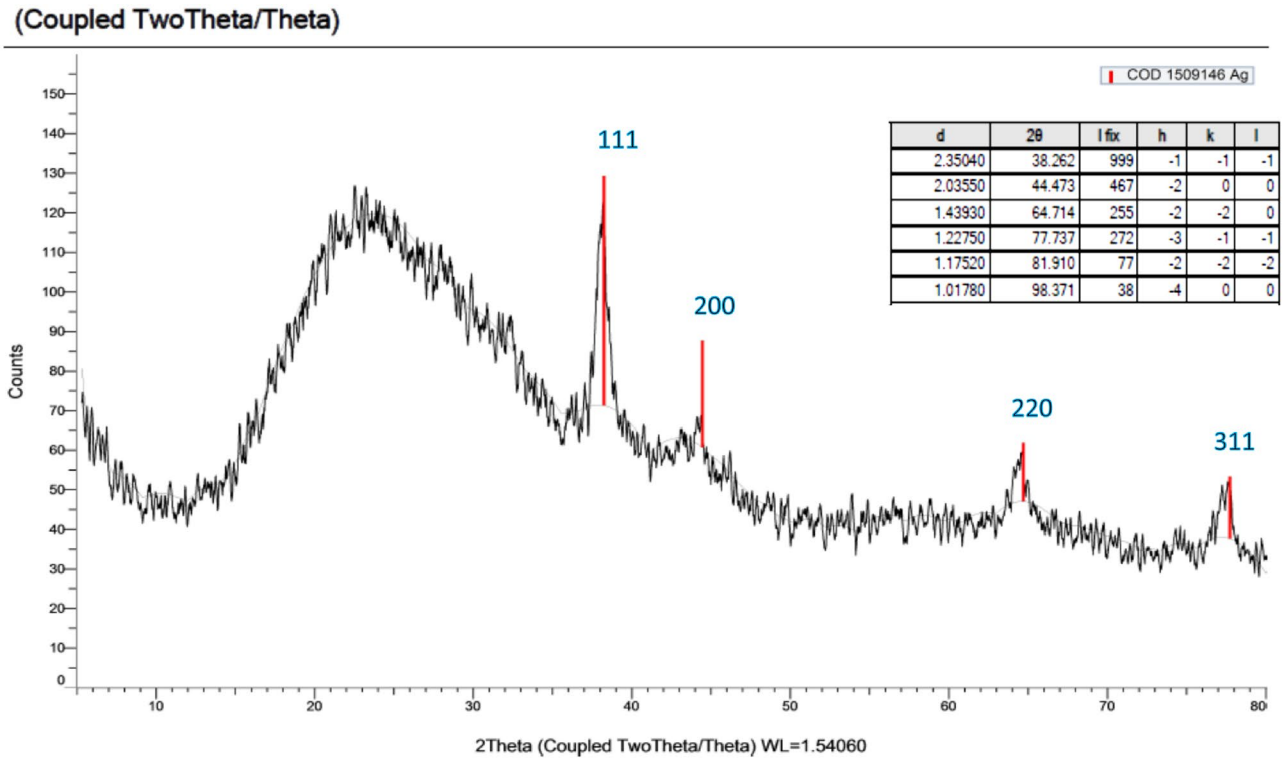

Figure 6. X-ray diffraction pattern of the biogenic LC-AgNPs.

Table 2. Cytotoxicity of LCTE and LC-AgNPs against MCF-7, HCT-116 HepG2 cancer cell lines after 72 h treatment.

Sample	IC_{50}on MCF-7 (µg/mL)	IC_{50} on HCT-116 (µg/mL)	IC_{50} on HepG2 (µg/mL)
LCTE	16.1 ± 2.96	26.34 ± 2.44	45.89 ± 3.68
LC-AgNPs	0.37 ± 0.05	0.35 ± 0.02	0.1 ± 0.003

The reported IC_{50}s are the average of triplicates ± standard deviation (SD).

at *m/z* of 627 and 611 and characteristic fragment ion at *m/z* of 302 and 287, respectively.

Characterization of the green-synthesized AgNPs

Physical observation

After 3 h of adding the LCTE to the prepared $AgNO_3$ solution, a physical observation of solution characters was performed. The clear solution turned into a dark murky colloidal solution. These findings demonstrated that the synthesis of LC-AgNPs and the reduction reaction had been completed.

UV-Vis spectroscopy

Because UV-Vis spectroscopy has a higher specificity for recognizing created nanoparticles than visible light, it was first utilized as the primary approach to validate the formation of nanoparticles. AgNPs have a distinctive optical reflectivity with a considerable impact on certain light wavelengths. When subjected to a coordinated oscillation of electrons, the unbound electrons within AgNPs resulted in the rise of an absorption band connected to the surface plasmon resonance (SPR). The degree of AgNP absorption may be influenced by a variety of variables, including the electrical medium, chemical microenvironment, particle shape, and particle size (Figure 2).

Fourier-transform infra-red (FTIR)

The identities of the functional reactive groups of the LCTE involved in the reduction process to produce LC-AgNPs have been investigated using spectroscopic FTIR. Peaks at 3385, 2922 and 1633 cm^{-1} reflect the OH, C aliphatic, and C=O of phenolics and flavonoids, respectively, while the peak at 1453 cm^{-1} represents aromatic components. The secondary OH groups of LCTE were validated by the peak at 1061 cm^{-1} (Figure 3).

High-resolution transmission electron microscope (HR-TEM)

HR-TEM has been used to study the eco-friendly AgNPs with LCTE as a reducing agent, showing the creation of spherical AgNPs with a mean size of 19.22 nm (Figure 4(A,B)). In addition, the crystalline character of LC-AgNPs was determined by the SAED pattern (Selected Area Electron Diffraction), (Figure 4(C)).

Scanning electron microscope (SEM)

The scanning electron microscope (SEM) is a potent tool for examining a material's surface image. It can depict the size of the particles, morphology, and distribution of the examined substance with pinpoint precision. It may also determine the morphological appearance of the item being analyzed, as well as whether it is micro- or nanoscale in size. The biogenic AgNPs were found to be spherical, with a tendency to combine, according to SEM examination (Figure 4(D–F)).

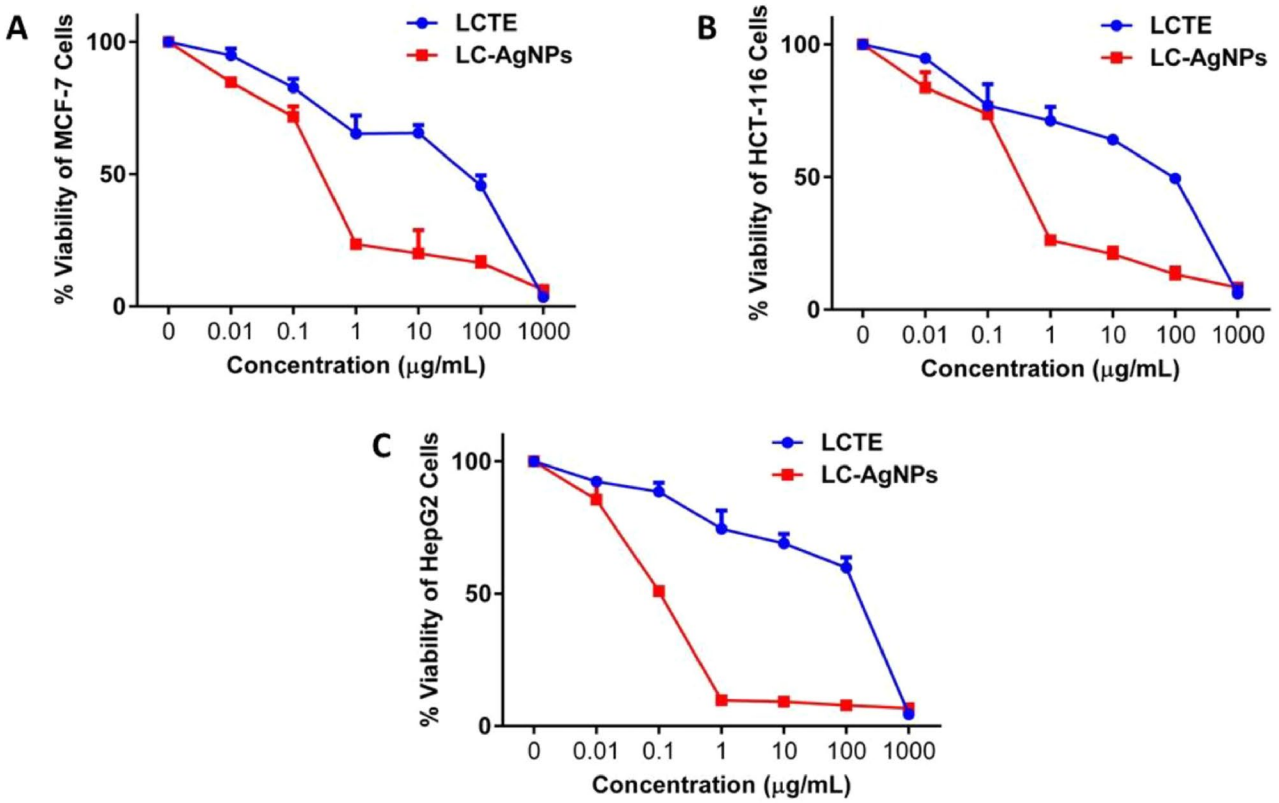

Figure 7. Cell viability of MCF-7 (A), HCT-116 (B), and HepG2 (C) cancer cells after treatment with LCTE and LC-AgNPs for 72 h. The data presented are the average ± standard deviation (SD).

Zeta potential and dynamic light scattering (DLS)

The zeta potential method was used to determine the charge of the biogenic LC-AgNPs. In this investigation, the surface charge zeta potential of LC-AgNPs was −14.3 mV. The negative charge highlighted the nanoparticles' stability (Figure 5(A)). The metallic shell size of 158.3 ± 4.37 nm of the biogenic LC-AgNPs was measured (Figure 5(B)).

X-ray diffraction (XRD)

Peaks appearing in the XRD chromatogram are fingerprinted to typical AgNPs formation at 38.262, 44.473, 64.714, and 77.737 on the 2 scale, which corresponded to 111, 200, 220 and 311 aircraft of Ag, respectively (Figure 6).

Cytotoxicity

Large efforts have been exerted in previous studies to evaluate the antitumor effect of LCTE and its bioactive components against obesity, cardiovascular diseases, diabetes, cancer, and the deadly metabolic syndrome [41]. Kiran et al. have reported LCTE wide spectrum anticancer effect against several tumour cell lines including H9C2, HepG2, A549 and Calu-1 cancer cell lines due to their high content of polyphenolics [78]. These findings take our interest to test LCTE for their antitumor activity against others such as human breast cancer (MCF-7), colorectal cancer (HCT-116), and hepatoma (HepG2) cell lines. To our knowledge, none of the existing research has investigated the use of LCTE to prepare biogenic AgNPs in an eco-friendly way. The cytotoxicity test of LCTE and LC-AgNPs treated samples was carried out to ascertain the impact of the prepared AgNPs using LCTE against MCF-7, HCT-116 and HepG2 cell lines using SRB assay. Cytotoxicity results are listed in Table 2 as computed IC_{50} values for pure LCTE and prepared LC-AgNPs and Figure 7 shows their cell viability against the 3 tested cell lines. LCTE showed quite good potency against the 3-cancer cell lines; IC_{50}=16.1, 26.34 and 45.89 µg/mL towards MCF-7, HCT-116 and HepG2, respectively (Table 2). The most potency was observed against MCF-7 while it was 1.5-fold lower against HCT-116. On the other hand, HepG2 was observed to be the least affected cell line when treated with pure LCTE; they showed the largest IC_{50} (45.89 µg/mL) (Figure 7(C)).

However, when LCTE was loaded on AgNPs, a fast significant drop in IC_{50} against HepG2 treated cells to 0.1 µg/mL of treatment was observed (Table 2 and Figure 7(C)). Also, LC-AgNPs remarkably lowered the percentage of the viable cells to about 20% at a concentration of 1 µg/mL on both MCF-7 and HCT-116 as shown in Figures 7(A,B) (IC_{50}=0.37 and 0.35 µg/mL, respectively). Such results verify the cytotoxic ability of the biosynthesized AgNPs using LCTE where it increases the cytotoxicity and lowers the viable cells more than 400 times when applied on HepG2 cells, about 75 times, and 43.5 times on HCT-116 and MCF-7 cell lines, respectively. The computed IC_{50} values (Table 2) were used for further investigations in the apoptosis and cell cycle analysis.

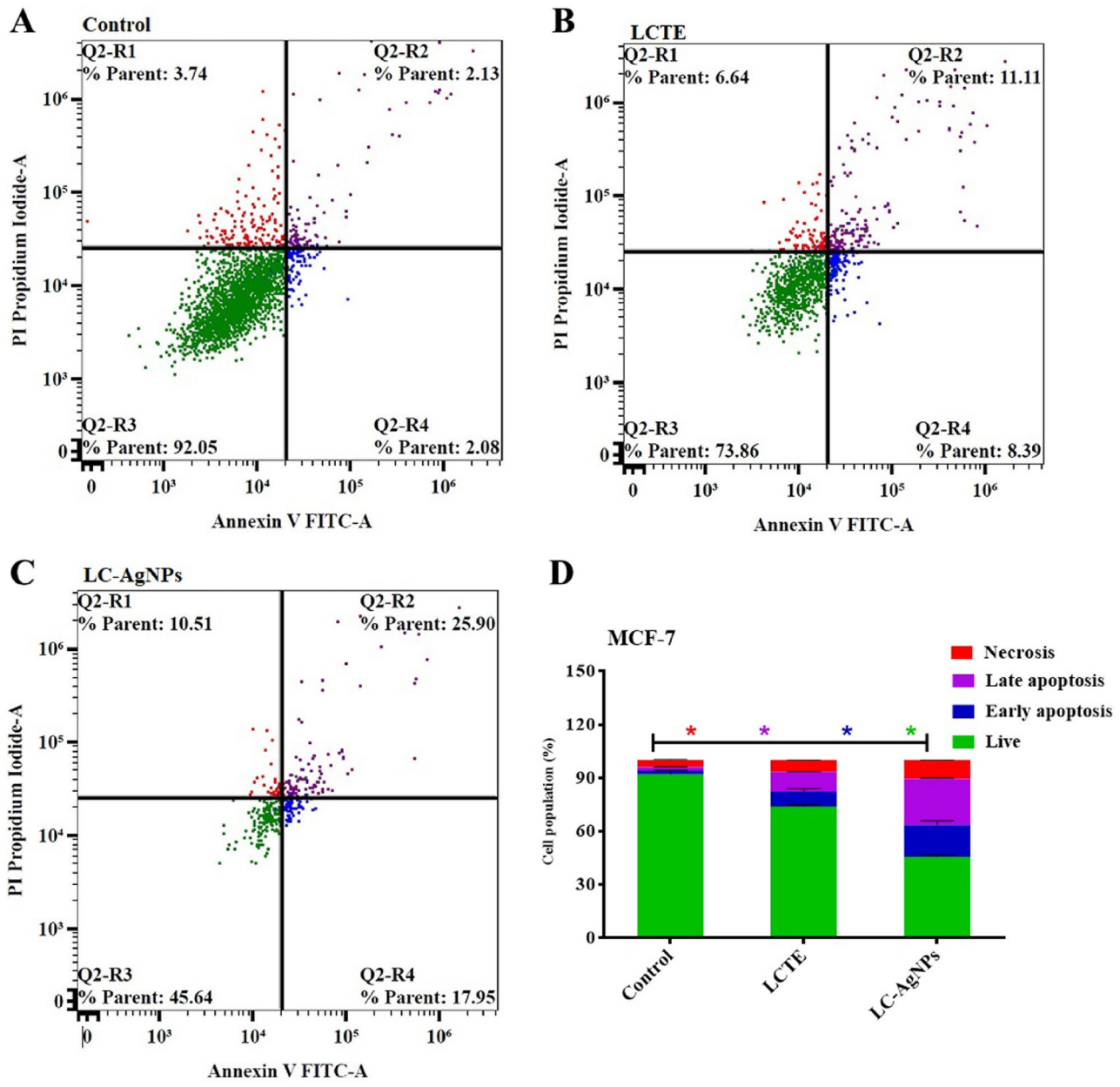

Figure 8. Apoptosis induction in MCF-7 cells using annexin-V/propidium iodide stain. Cytograms showing MCF-7 cells nontreated (negative control) (A), treated MCF-7 cells with LCTE (16.1 µg/mL, 48 h) (B), treated MCF-7 cells with LC-AgNPs (0.37 µg/mL, 48 h) (C), and illustration of the outcomes of the apoptosis analysis (D).

Apoptosis assay

SRB cytotoxicity assay revealed that the LC-AgNPs enhanced the cytotoxic effect of LCTE on the 3 cancer cell lines. In this context, further evaluation was needed to examine how cell death occurred. The cancer cell lines were treated with the pre-calculated IC_{50} values for LCTE and LC-AgNPs for 48 h. For negative control, non-treated cells were utilized to calculate the percentages of necrotic and apoptotic cell populations via annexin-FITC/propidium iodide (AV/PI). Figures 8–10 display the cell apoptosis assay results on MCF-7, HCT-116 and HepG2, respectively.

Results, as shown in Figure 8, indicated that treating MCF-7 cells with LCTE caused apoptosis and induced a significant 20% reduction in cell viability. In addition, the sub-population exhibiting early apoptosis (AV+/PI–) increased to 8.39%, the average count of the late apoptotic sub-population (AV+/PI+) reached 11.11%, and necrosis increased (less than twice as much as the control). The outcomes demonstrated that the LCTE successfully induced apoptosis, substantially late apoptosis, in MCF-7 cells (Figure 8(B)). When pure LCTE was applied to HCT-116 cells, similar outcomes were seen; these cells sub-populated in early apoptosis (AV+/PI–) is about 5.34%, and late apoptotic sub-population (AV+/PI+) percentage was 8.32% (4 folds more than the negative control) and a necrotic effect was also observed (about 2-fold more than that of the control) (Figure 9(B)). Regarding HepG2 cell line treatment with pure LCTE, a remarkable increase in both early and late apoptosis sub-population percentages were observed; where it reached 14.89 and 22.75% which is 6.9 and 9.6

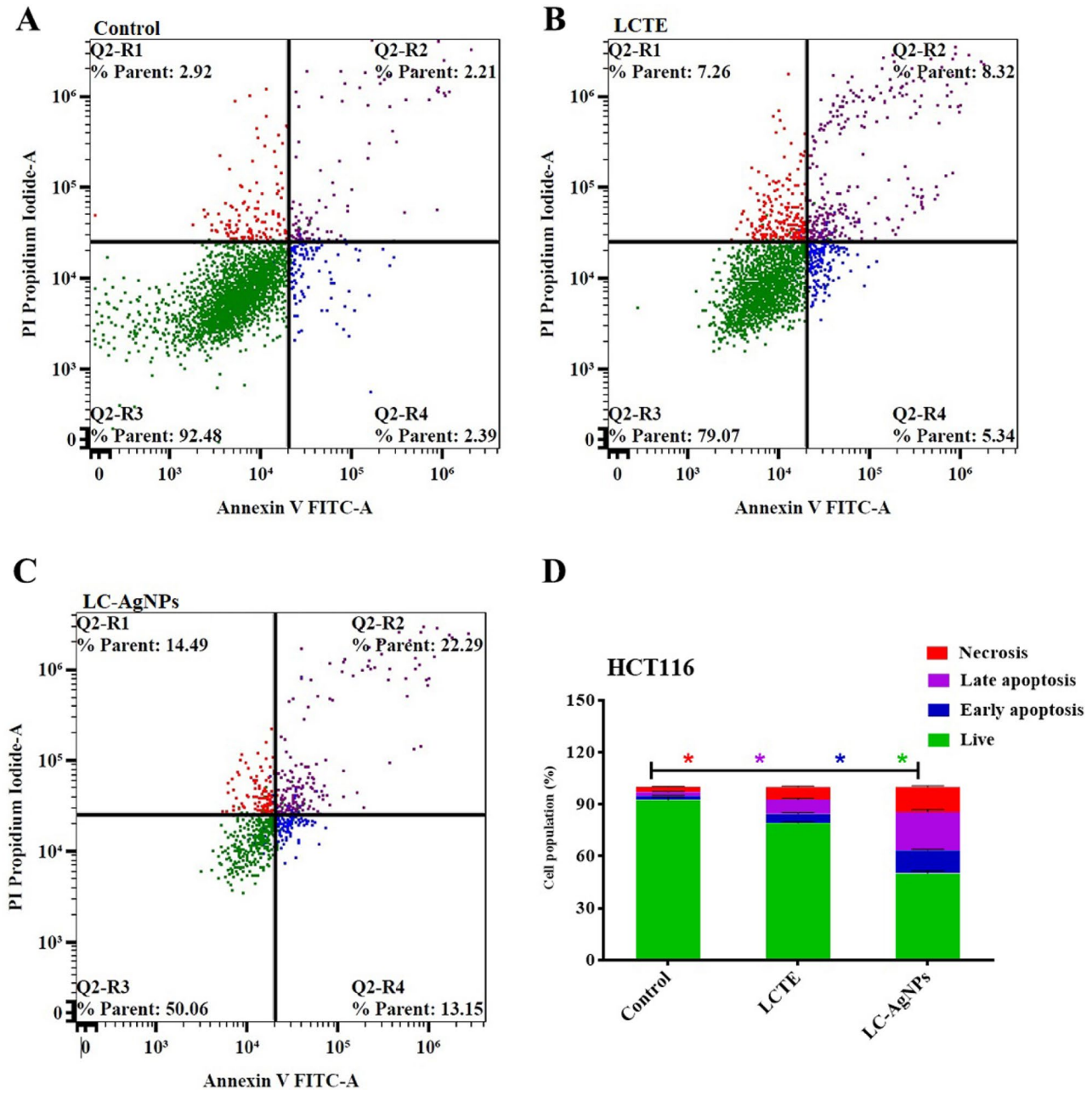

Figure 9. Apoptosis induction in HCT-116 cells by annexin-V/propidium iodide stain. Cytograms showing HCT-116 cells nontreated (negative control) (A), treated HCT-116 cells with LCTE (26.34 µg/mL, 48 h) (B), treated HCT-116 cells with LC-AgNPs (0.35 µg/mL, 48 h) (C), and illustration of the outcomes of the apoptosis analysis (D).

times relative to the untreated regulation for both early and late apoptosis, respectively (Figure 10(B)). It was also able to increase the percentage of necrotic cell population 3 folds than untreated HepG2 cells.

Accordingly, LCTE is suggested to induce its cytotoxic effect via an apoptotic pathway, mainly late apoptosis. This confirms the apoptotic pathway of LCTE reporting the involvement of increased caspase 3, 8 and 9 activity triggering late apoptosis in nasopharyngeal carcinoma cell lines [79]. Another study also reported that different tumour cell lines (A549, Calu-1, H9C2, Caco2, C2C12 and SK-N-BE-2 cells) exhibit significant apoptosis through suppressing oxidative stress-responsive genes and hence inhibiting cancer cell proliferation [78].

LC-AgNPs tested against the 3 cell lines reduced the cell viability by 28.22, 29.01, and 12.8% against MCF-7, HCT-116 and HepG2 cell lines, respectively compared to those treated with LCTE alone (Figures 8(C), 9(C), and 10(C)). The percentage of late apoptotic sub-population in MCF-7 treated with LC-AgNPs increased to 25.9% which is 2.3 times higher than the treatment with LCTE alone and more than 11 times higher than the negative control while the early apoptosis sub-population percentage increased to 17.95% which 2 and 8.5 times more than pure LCTE treated and untreated MCF-7 cells, respectively. On the other hand, a little rise in necrotic sub-population percentage was noticed (Figure 8(C))

Figure 9(C) showed a significant decrease in HCT-116 viable cells when treated with LC-AgNPs where they

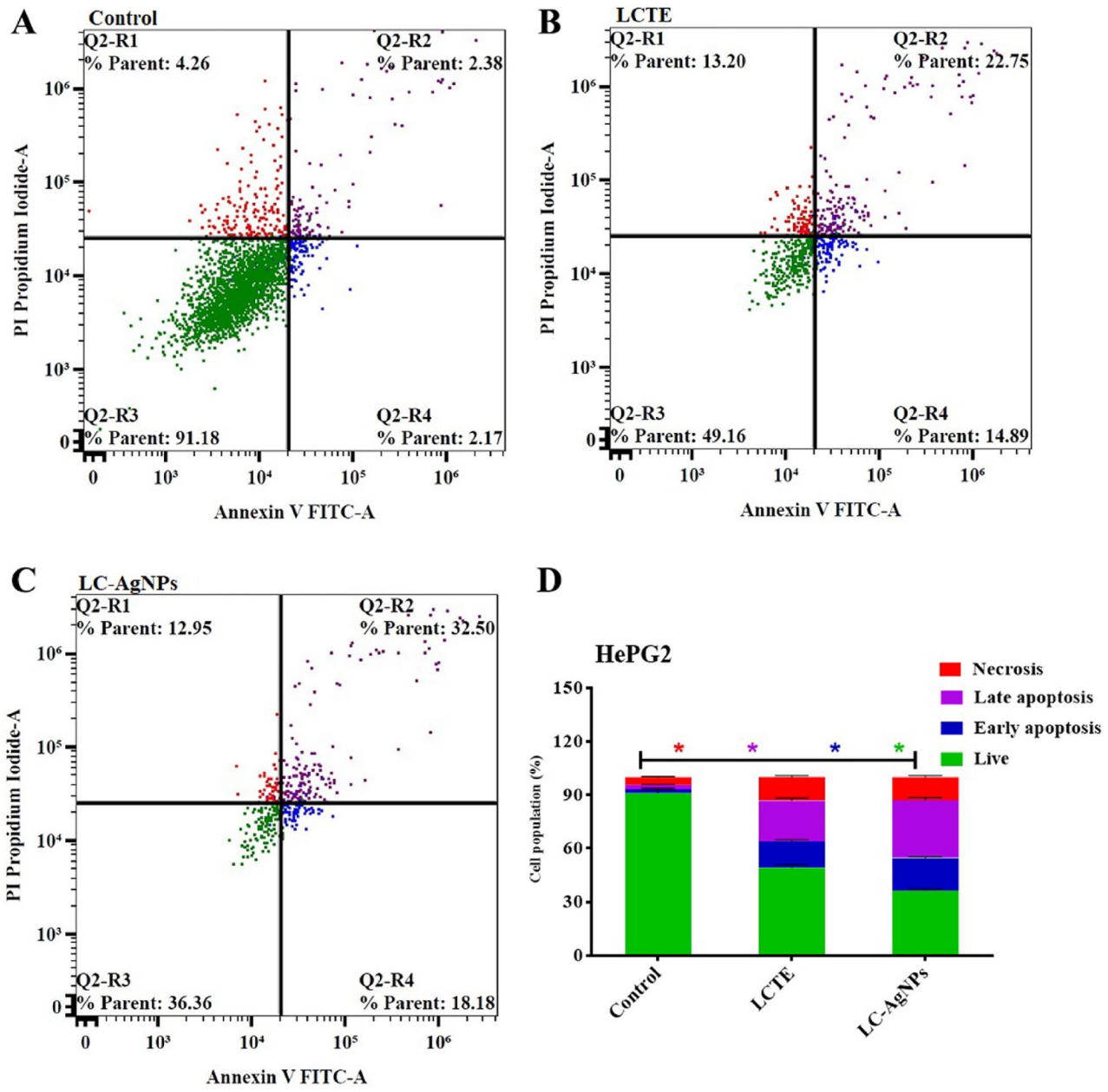

Figure 10. Apoptosis induction in HepG2 cells by annexin-V/propidium iodide stain. Cytograms showing HepG2 cells nontreated (negative control) (A), treated HepG2 cells with LCTE (45.89 µg/mL, 48 h) (B), treated HepG2 cells with LC-AgNPs (0.1 µg/mL, 48 h) (C), and graphical illustration of the outcomes of the apoptosis analysis (D).

decreased to 50.06% which is about two-fold less than the untreated ones. Late apoptotic sub-populations were noted to be the highest population percentage (22.29%), whereas early apoptotic and necrotic populations were equally affected (13.15 and 14.49%, respectively). HepG2 cell lines were the most affected cancer cell lines with LC-AgNPs treatment through inducing late apoptosis 32.5%, while not much difference was observed in early apoptosis and necrosis compared to treating HepG2 with pure LCTE (Figure 10(C)).

The observed results show that AgNPs mainly exert their anticancer activity in breast, colorectal, and hepatic cancer cell lines by inducing the apoptotic pathways (early and late apoptosis equally). This aligns with the reported findings [80].

Cell cycle analysis

To study the percentage of cell proliferation indicating the cell cycle phase interference, a cell cycle analysis test was utilised after treating the 3 cancer cell lines with both LCTE and LC-AgNPs for 48 h. As shown in Figure 11, the highest observed induction of cell arrest in the MCF-7 cell line was observed at G1-phase with 1.58-fold and 1.59-fold (67.1 and 67.3%) when treated with LCTE and LC-AgNPs, respectively compared to 42.4% for control. At the S and G2-cell-cycle phases, the percentage of cells decreased with both treatments. These results affirmed that LCTE induced G1 phase arrest in breast cancer. This could be attributed to the remarkable increase in ROS after lectins treatment in addition to caspase-3 activation [81]. Also, green synthesised AgNPs

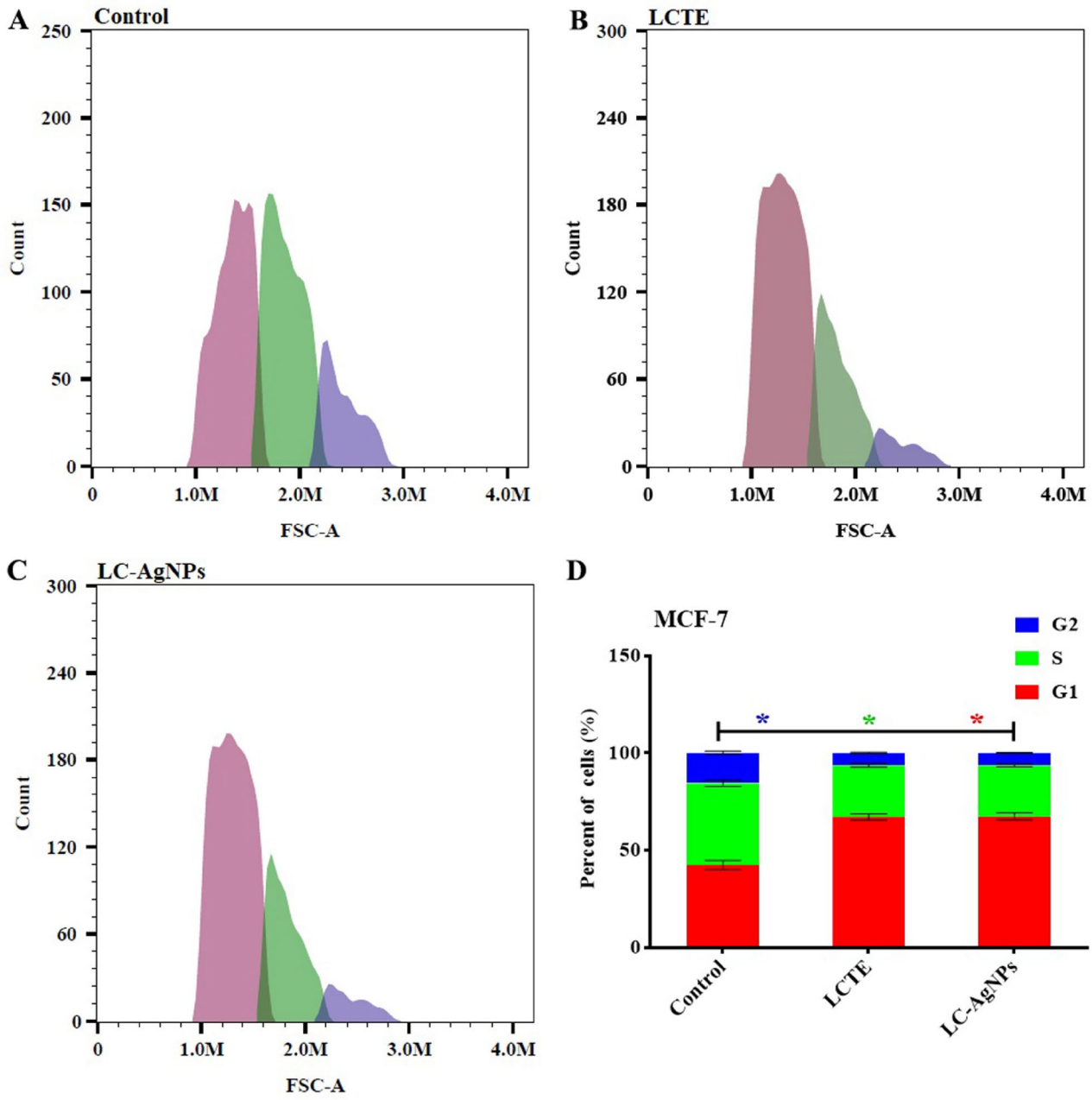

Figure 11. Cytogram showing cell cycle analysis of untreated MCF-7 cells (control) (A), LCTE-treated MCF-7 cells (B), LC-AgNPs treated MCF-7 cells (C), and proportion of the MCF-7 cell population at each stage of the cell cycle (D).

treatment resulted in G0/G1 phases arrest of the cell cycle arrest of the examined breast cancer cells.

In colorectal carcinoma (HCT-116) cell lines, no difference was observed in any cell cycle phase between the LCTE treatment and the negative control (Figure 12). Previous research reported that LCTE induced HT-29 cell arrest in the G0/G1 phase through phosphorylating P53 in colon cancer [82]. When HCT-116 cells were treated with LC-AgNPs, a notable elevation in the G1 phase population was reported. These findings confirm our reported analysis of the MCF-7 cell line.

On the contrary, the HepG2 cell line showed a significant increase in the G2 cell arrest population upon treatment with both LCTE and LC-AgNPs (34.6% for both) compared to 22.1% in negative control with no significant change in S populations (Figure 13). Although there no reported data existed for the use of lentil extract against hepatocarcinoma, studies suggested that lentil extract exhibited an anti-hepatotoxic effect owing to its antioxidant activity, i.e. its ability to decrease ROS levels [83].

Antimicrobial activity

Antibacterial activity

The two bacterial isolates showed a high resistance against ciprofloxacin antibiotic. Although LCTE extract did not show any effect against the strong biofilm-forming *Klebsiella pneumoniae* isolate and the extensive drug-resistant *Acinetobacter baumannii* isolates, LC-AgNPs showed high activity against both (Table 3 and Figure 14).

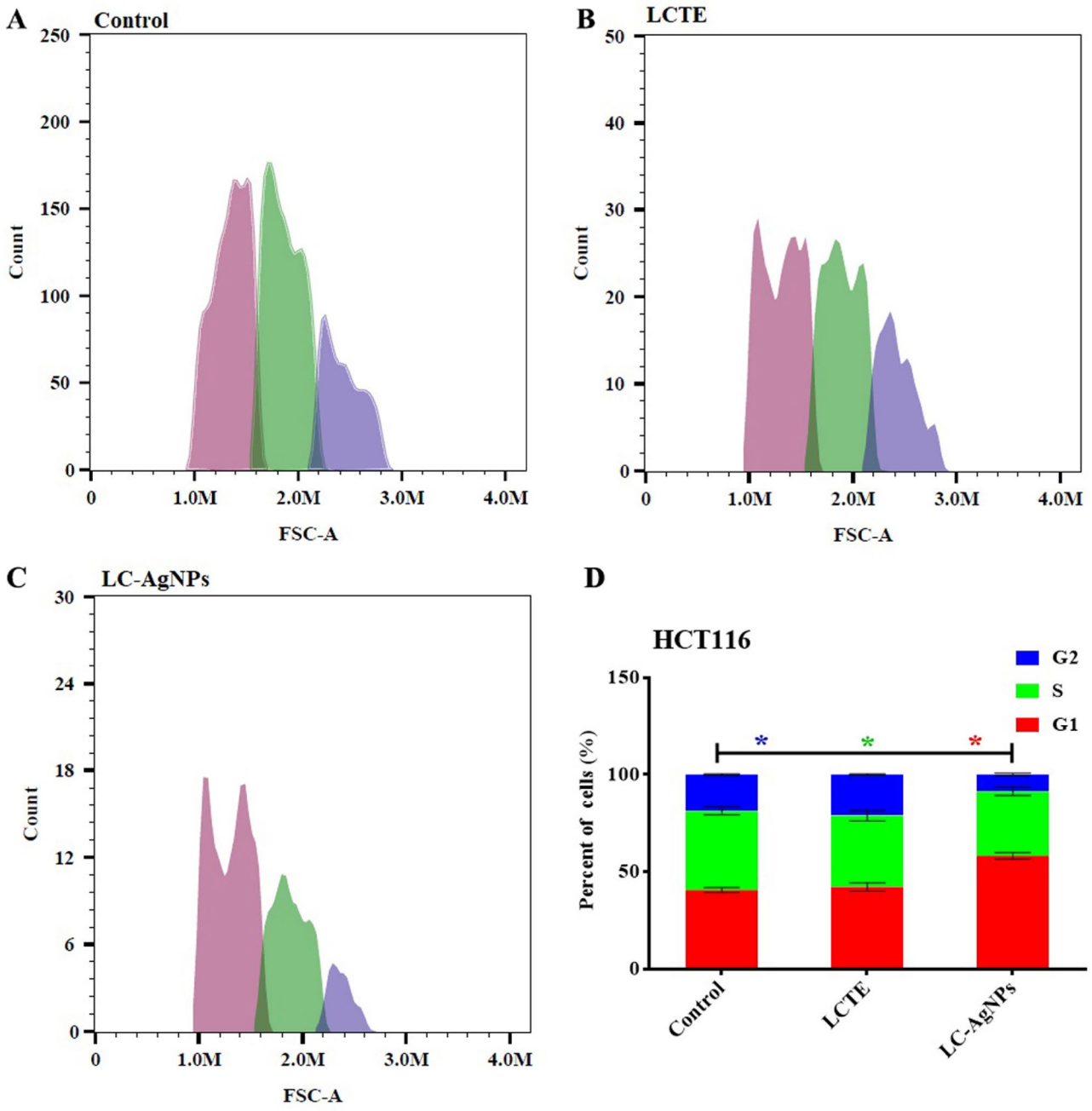

Figure 12. Cytogram showing cell cycle analysis of untreated HCT116 cells (control) (A), LCTE-treated HCT-116 cells (B), LC-AgNPs treated HCT-116 cells (C), and proportion of the HCT-116 cell population at each stage of the cell cycle (D).

Molecular docking

The anticancer activity of LCTE active major classes was assessed by examining their binding affinities against the Bcl-2 protein. As shown in Table 4, Figures 15 and S2, all the 17 reported major classes have shown good binding affinities with significant binding energies ($-4.05 < \Delta G < -7.97$ Kcal/mol). Kaempferol-3-O-robinoside-7-O-rhamnoside was shown to be the best hit having the ability to bind to Bcl-2 groove forming two tightly bound H-bonds with 2 key residues: Glu95 and Asp99. Two main types of interactions are reported with all active constituents which are pi-pi interactions and H-bonds in addition to salt-bridge which is mainly formed with Arg105.

Better binding interactions are shown for LCTE active constituents with IspC. As shown in Table 5, Figures 16 and S3, high binding energies are reported in range ($-6.19 < \Delta G < -10.29$ Kcal/mol). Catechin gallate is found to be the most fitted hit where it can form 3 H-bonds and 2 salt bridges; one of them with the co-crystallized Mg ion in the pocket. Mg ion is found to be able to form salt-bridge or metal acceptor interaction with most structures. Another key interaction is the pi-sulphur interaction which can be formed with Met in the pocket. A large number of H-bonds, salt bridges, and hydrophobic interactions formed between LCTE active structures and IspC active pockets are indications of their antibacterial activity.

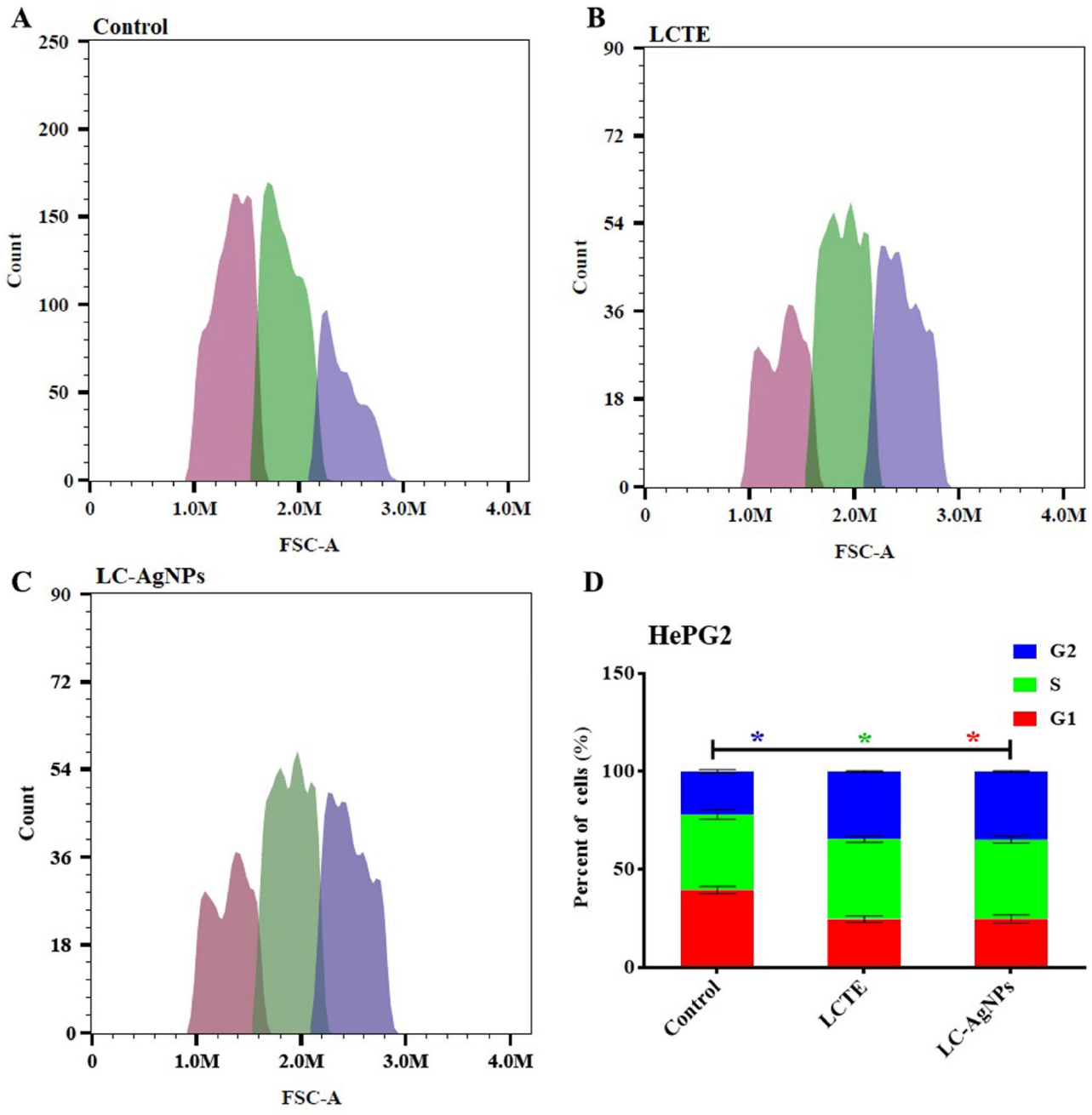

Figure 13. Cytogram showing cell cycle analysis of untreated HepG2 cells (control) (A), LCTE-treated HepG2 cells (B), LC-AgNPs treated HepG2 cells (C), and proportion of the HepG2cell population at each stage of the cell cycle (D).

Table 3. Antimicrobial screening of LCTE and LC-AgNPs against *Klebsiella pneumoniae* and *Acinetobacter baumannii*.

Sample	Bacteria	Zone of inhibition
LC-AgNPs	*Klebsiella pneumoniae* (K21)	24 ± 1.67 mm
	Acinetobacter baumannii (M18)	25 ± 1.29 mm
LCTE	*Klebsiella pneumoniae* (K21)	No inhibition
	Acinetobacter baumannii (M18)	No inhibition

Zones of inhibition are displayed as the average of triplicates ± standard deviation (SD).

LCTE was used in capping AgNPs and the formulated NPs were found to possess both anti-cancer and antibacterial effects. A docking study was carried out to investigate the binding affinity of the produced NPs in potential cavities in both protein targets; Bcl-2 and IspC. Good binding affinity (−0.19 Kcal/mol) is reported for both complexes which suggests a high potency. Figure 17 shows that AgNP was able to bind to an allosteric pocket in Bcl-2 protein (shown in magenta sticks) away from the co-crystallized ligand (represented in cyan sticks) active pocket. The allosteric pocket was composed of His20, Leu23, Ser24,

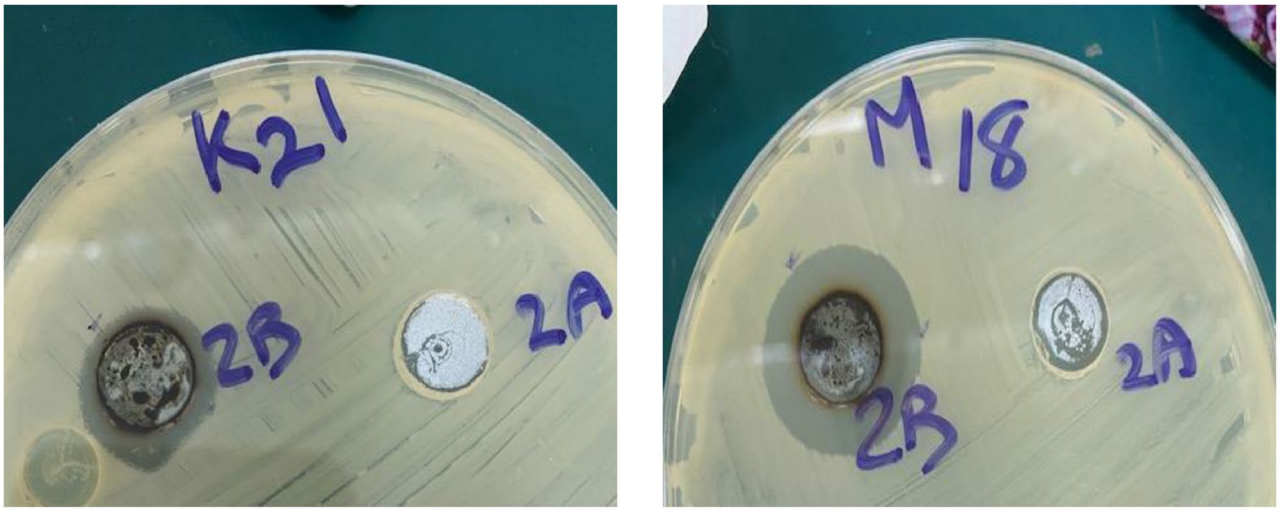

Figure 14. Zone of inhibition of LCTE and LC-AgNPs against *Klebsiella pneumoniae* and *Acinetobacter baumannii*.

Table 4. Compounds IDs, bonded residues with Bcl-2 protein, and their binding energies with Bcl-2 protein.

Compound	Bonded residues	Binding energy (Kcal/ mol)
Vanillic acid glucoside	Asp70, Glu95, Arg105	−5.54
3, 4-Dihydroxybenzoic acid	Phe63	−4.05
Epigallocatechin	Tyr67, Phe71, Glu95, Arg105	−4.90
Catechin gallate	Asn102, Arg105, Ala108	−6.07
Esculin	Phe71, Asp99	−5.60
Kaempferol 3-*O*-arabinoside	Glu95, Arg105	−6.19
Kaempferol-3-*O*-rhamnoside	Phe63, Tyr67, Glu95, Asp99, Arg105	−6.25
kaempferol-3,7-*O*-*bis*-rhamnoside	Asp70, Glu95, Asp99	−7.12
kaempferol-7-*O*-rutinoside	Gly77, Arg88, Glu95, Asp99	−6.90
Kaempferol-3-*O*-robinoside-7-*O*-rhamnoside	Glu95, Asp99	−7.97
Eriodictyol	Tyr67, Phe71, Arg105	−4.95
Hesperetin	Phe63, Arg105	−5.38
Datiscin	Glu73, Asp99	−6.91
Apigenin	Asp99, Arg105	−4.88
Diosmetin	Asp70, Arg105	−5.19
Quercetin-3-D-xyloside	Asp70, Glu95, Arg105	−6.48
Isorhamnetin 7-rhamnoside	Asn102, Arg105	−6.57

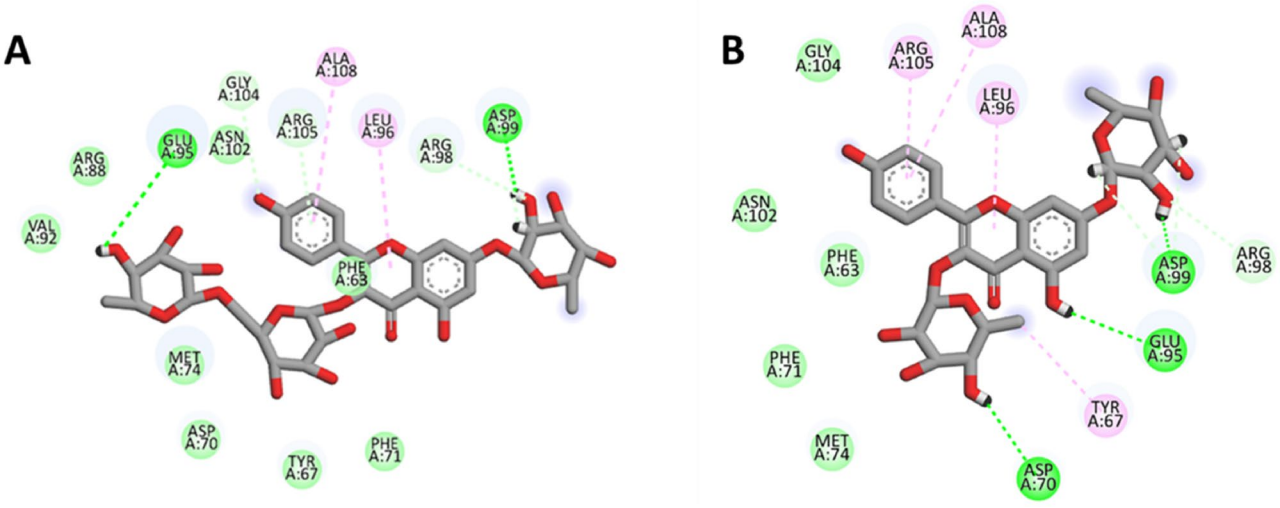

Figure 15. Representative compounds' 2D interaction with Bcl-2 protein. (A) Kaempferol-3-O-robinoside-7-O-rhamnoside forming tightly bound H-bonds with: Glu95 and Asp99. (B) Kaempferol-3 7-O-bis-rhamnoside forming tightly bound H-bonds Asp70, Glu95 and Asp99.

Glu29 and Trp30. Similarly, Figure 18 shows that AgNP was also able to bind to a pocket in IspC protein (shown in magenta sticks) away from the main active site (represented in green sticks). Eight residues were involved in this potential interaction: Ile342, Leu343, Ala346, Asn347, Val368, Thr371, Leu372 and Ala393.

Kaempferol-3-*O*-robinoside-7-O-rhamnoside and Quercetin-3-D-xyloside were chosen as the best two LCTE active

Table 5. Compounds IDs, bonded residues with IspC protein and their binding energies.

Compound	Bonded residues	Binding energy (Kcal/ mol)
Vanillic acid glucoside	Ser21, Ala109, Ala132, Ser160	−8.37
3,4-Dihydroxybenzoic acid	Lys134, Ser160, Lys236, Mg	−8.67
Epigallocatechin	Ile22, Arg47, Ala109, Ile110, Glu135	−6.77
Catechin gallate	Glu135, Asp159, Gly223,, Lys134, Mg	−10.29
Esculin	Asp159, Glu161, Ser194, Asn235, Ile226, Mg	−7.33
Kaempferol 3-*O*-arabinoside	Ser21, Ala132, Gly223, Arg24, Arg47	−7.40
Kaempferol-3-*O*-rhamnoside	Ala132, Ser160, Lys236, Met222, Ser221	−7.83
kaempferol-3 7-*O*-*bis*-rhamnoside	Arg47, Ala109	−7.52
kaempferol-7-*O*-rutinoside	Arg47, Ala109, Ile110, Ala132, Glu135, Glu352, Mg	−9.39
Kaempferol-3-*O*-robinoside-7-*O*-rhamnoside	Ser46, Arg47, Ala109, Ile110, Glu352	−9.27
Eriodictyol	Ser21, Ala109, Asn133, Glu135, Gly223, Met222	−7.17
Hesperetin	Gly17, Arg47, Ala109, Glu135, Gly223	−6.85
Datiscin	Arg47, Ala109, Asp159, Ser160, Gly223, Gln224	−8.55
Apigenin	Ala109, Asn133, Glu135, Ser160, Gly223, Trp220, Met284	−6.63
Diosmetin	Arg47, Ile110	−6.19
Quercetin-3-D-xyloside	Ser21, Glu135, Lys134, Asn235, Lys236, Met284, Mg	−9.9
Isorhamnetin 7-rhamnoside	Thr19, Ser21, Arg47, Ala109, Ile110, Ser160, Lys134Met22	−8.10

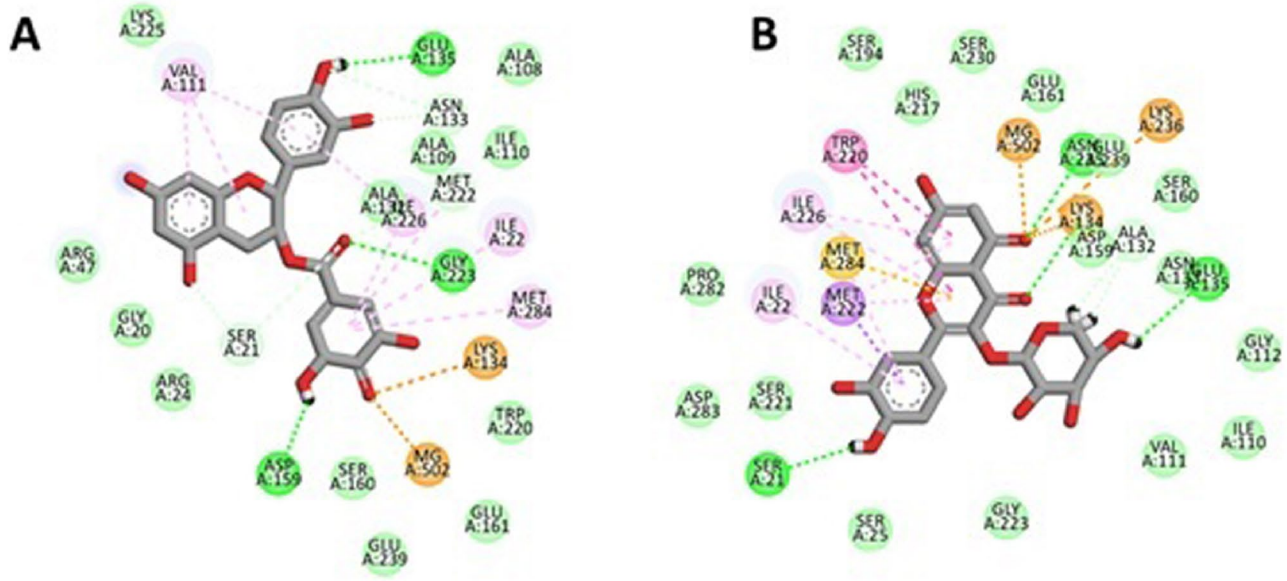

Figure 16. Representative compounds' 2D interaction with IspC protein. Catechin gallate (A), Quercetin-3-D-xyloside (B).

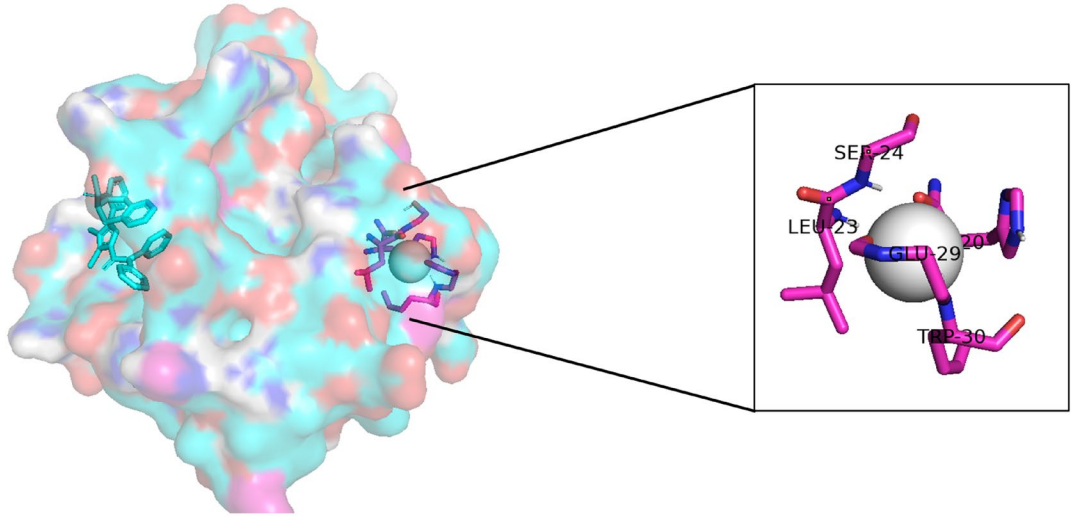

Figure 17. The 3D structure of BcL-2 targets showing the binding interaction of AgNP in the allosteric pocket (shown in magenta sticks).

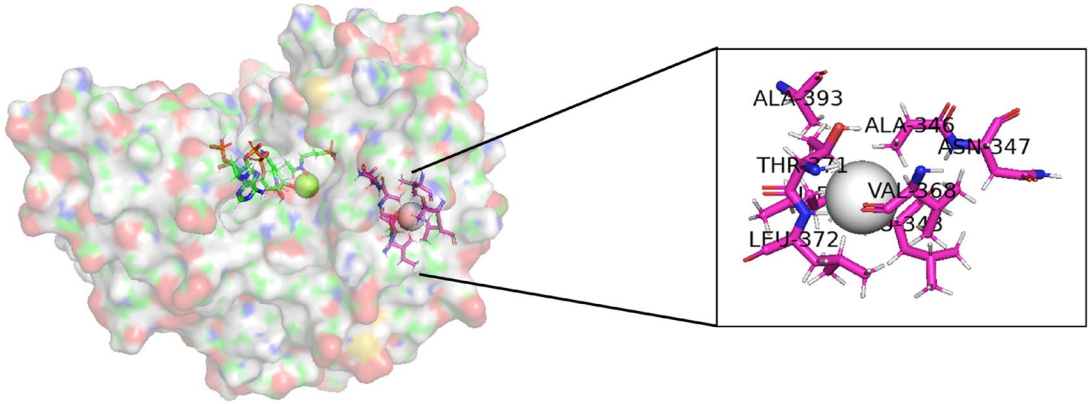

Figure 18. The 3D structure of the IspC target showing the binding interaction of AgNP in the allosteric pocket (shown in magenta sticks).

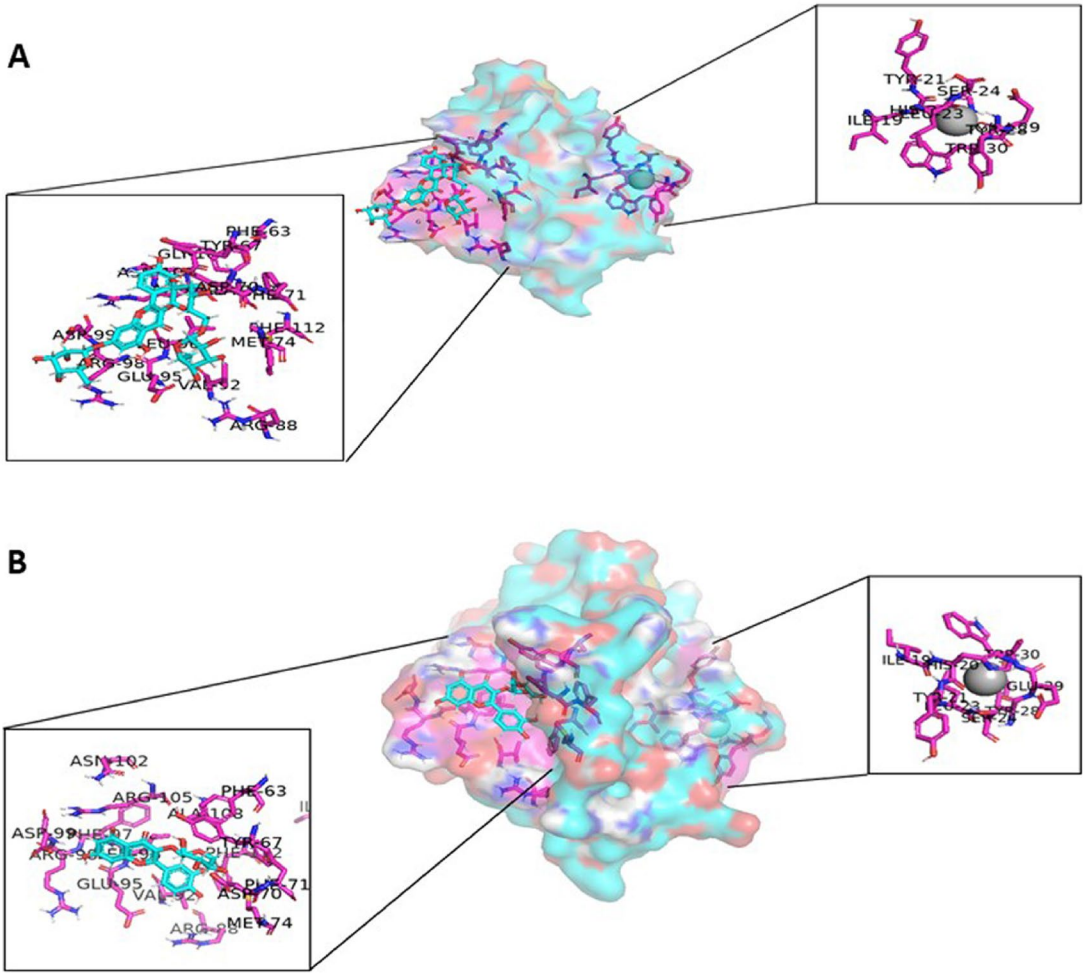

Figure 19. 3D Structure of BcL-2 target showing the synergetic binding of AgNP and kaempferol-3-O-robinoside-7-O-rhamnoside (A) and AgNPs and quercetin-3-D-xyloside (B) where the binding pocket residues are shown in magenta sticks.

constituents capable of inhibiting both Bcl-2 and IspC targets. So, the synergetic binding of these two hits with AgNPs was visualized in Figures 19 and 20. Either Kaempferol-3-*O*-robinoside-7-*O*-rhamnoside or Quercetin-3-D-xyloside were able to bind to the enzyme's active pocket at the same time as the allosteric binding of AgNPs. This explains our previous finding of the high cytotoxic effect of LC-AgNPs that reached between 43.5 to 400 folds on different cancer cell lines than that of LCTE alone.

Conclusions

- Introducing a simple, safe, eco-friendly, and low-cost technique for the preparation of silver nanoparticles using *Lens culinaris L.* extract as a bio-reduction agent (green synthesis).
- LC-MS analysis of *Lens culinaris* identified twenty-two compounds of different chemical classes.

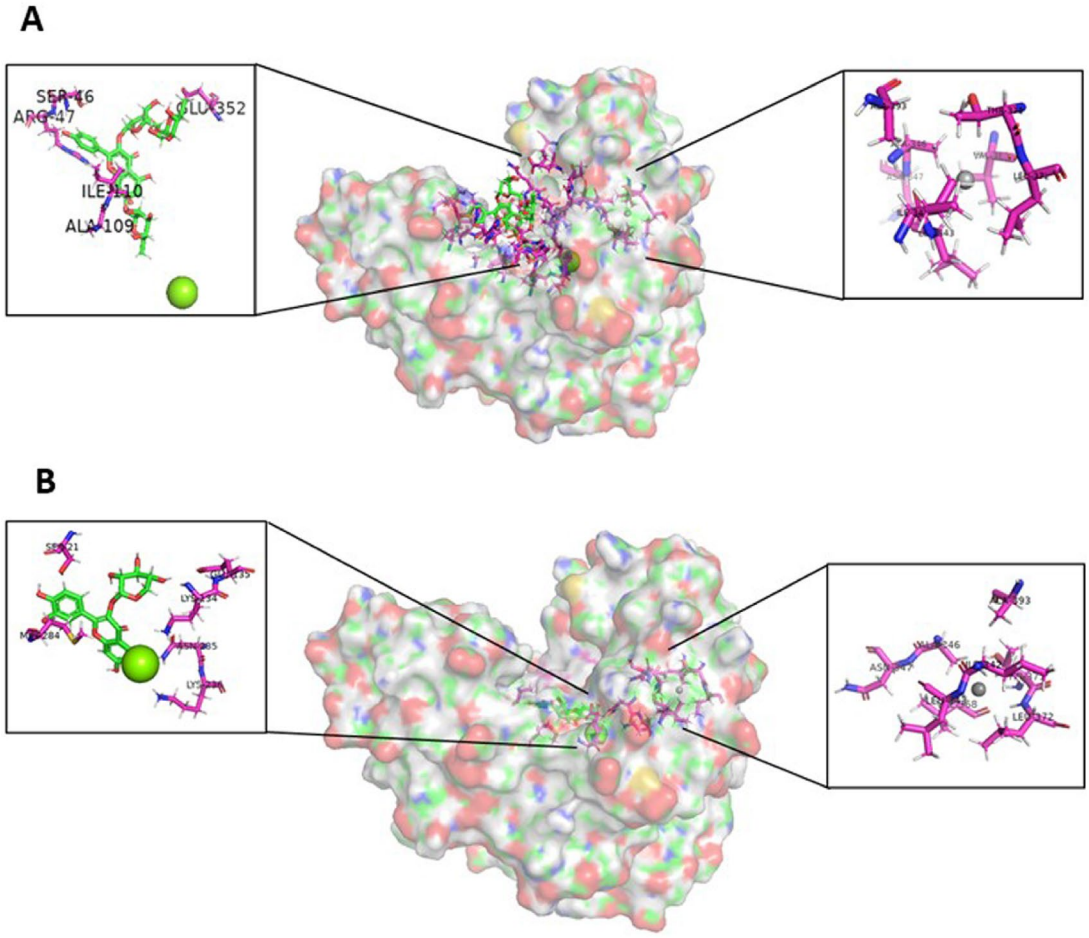

Figure 20. The 3D structure of the IspC target showing the synergetic binding of AgNP and kaempferol-3-O-robinoside-7-O-rhamnoside (A) and AgNPs and quercetin-3-D-xyloside (B) where the binding pocket residues are shown in magenta sticks.

- Shifting in FTIR spectrum peaks revealed the important role of the various functional groups of *Lens* secondary metabolites for capping and stabilization.
- Ag nanoparticles' spherical shape and FCC crystallinity were proved through HR-TEM and XRD with a 19.22 nm size on average.
- The Zeta potential value of AgNPs was −14.3mV indicating their stability.
- LCTE potentiated the cytotoxic activity of AgNPs against MCF-7, HCT-116, and HepG2 cancer cell lines.
- LCTE induced G1 phase arrest and AgNPs-LCTE increased G0/G1 phases in breast cancer. Meanwhile, both LCTE and LC-AgNPs increased G2 cell arrest in HepG2.
- AgNPs mainly exerted their anticancer activity by inducing the apoptotic pathways via activation of caspase-3, down-regulation of Bcl2, and up-regulation of Bax and p53.
- Kaempferol-3-O-robinoside-7-O-rhamnoside and Quercetin-3-D-xyloside were the best 2 LCTE active constituents capable of inhibiting both Bcl-2 and IspC targets.
- Kaempferol-3-O-robinoside-7-O-rhamnoside and Quercetin-3-D-xyloside were also able to bind to the enzymes active pocket at the same time of the allosteric binding of AgNPs. This entails the high cytotoxic effect of LC-AgNPs that reached between 43.5 to 400 folds on different cancer cell lines compared to that of LCTE alone.
- LCTE-AgNPs showed strong activity against *Klebsiella pneumoniae* and *Acinetobacter baumannii* compared to LCTE.

Future recommendations

Further research is needed to unveil the effect of *Lens culinaris* phytochemicals on the physicochemical parameters of the biogenic AgNPs for the optimisation of their biological activities. Moreover, pharmacological assessments could be conducted on such biogenic AgNPs compared to the original extracts and their safety must be assessed before their clinical investigation.

Acknowledgements

The authors thank the Deanship of Scientific Research at King Khalid University for funding this work through large Groups (Project under grant number R.G.P. 2/ 217 /44). The authors thank Prof. Dr. Reem Arafa's research group for offering a great scientific reference that helped a lot in the methodology section. The authors thank Prof. Dr Seham Elhawary for providing scientific guidance for this research. The authors appreciate

Dr Sherif Ashraf Fahmy lecturer in School of Life and Medical Sciences, University of Hertfordshire Hosted by Global Academic Foundation, for his support in the revision stage.

Ethical approval

No ethics approval was required as the study did not include humans or animals. All authors have read and agreed to the published version of the manuscript.

Author contributions

Conceptualisation, Heba W. Alhamdi, Fatma Alzahraa Mokhtar, Ali A. Shati, Serag Eldin I. Elbehairi, Lamiaa I. Fahmy, Mohammad Y. Alfaifi, Nada K. Sedky and Heba A. Fahmy; Data curation, Serag Eldin I. Elbehairi; Investigation, Fatma Alzahraa Mokhtar, Serag Eldin I. Elbehairi, Lamiaa I. Fahmy and Mohammad Y. Alfaifi; Resources, Heba W. Alhamdi and Mohammad Y. Alfaifi; Software, Fatma Alzahraa Mokhtar; Supervision, Fatma Alzahraa Mokhtar; Validation, Ali A. Shati, Nada K. Sedky, Fouad Lamghari Ridouane, and Heba A. Fahmy; Writing – original draft, Heba W. Alhamdi, Ali A. Shati, Serag Eldin I. Elbehairi, Lamiaa I. Fahmy, Mohammad Y. Alfaifi, Nada K. Sedky and Heba A. Fahmy; Writing – review & editing, Fatma Alzahraa Mokhtar, Fouad Lamghari Ridouane, and Heba A. Fahmy.

Disclosure statement

No potential conflict of interest was reported by the author(s).

Funding

This work has been funded by King Khalid University [Project under grant number R.G.P. 2/ 217 /44].

ORCID

Fatma Alzahraa Mokhtar http://orcid.org/0000-0002-6909-7440
Nada K. Sedky http://orcid.org/0000-0002-2359-3799

Data availability statement

The authors confirm that the data supporting the findings of this study are available within the article and its supplementary materials.

References

[1] Selvan ST, Tan TTY, Yi DK, et al. Functional and multifunctional nanoparticles for bioimaging and biosensing. Langmuir. 2010;26(14):11631–11641. doi: 10.1021/la903512m.
[2] Velhal K, Barage S, Roy A, et al. A promising review on cyclodextrin conjugated paclitaxel nanoparticles for cancer treatment. Polymers. 2022;14(15):3162. doi: 10.3390/polym14153162.
[3] Naik HS, Sah PM, Dhangade M, et al. Synthesis of a silica matrix with ZnO nanoparticles for the fabrication of a recyclable photodegradation system to eliminate methylene blue dye. Green Process Synth. 2023;12(1):20230157. doi: 10.1515/gps-2023-0157.
[4] Sharma S, Kumar S, Bulchandini B, Taneja S, Banyal S. Green synthesis of silver nanoparticles and their antimicrobial activity against gram positive and gram negative bacteria. Int J Biotechnol Bioeng Res. 2013;4(7):711–714.
[5] Azharudeen AM, Roy A, Karthiga R, et al. Ultrasensitive and selective electrochemical detection of dopamine based on CuO/PVA nanocomposite-modified GC electrode. Int J Photoenergy. 2022;2022(1):1–9. doi: 10.1155/2022/8755464.
[6] Onitsuka S, Hamada T, Okamura H. Preparation of antimicrobial gold and silver nanoparticles from tea leaf extracts. Colloids Surf B Biointerfaces. 2019;173:242–248. doi: 10.1016/j.colsurfb.2018.09.055.
[7] Sedky NK, Mahdy NK, Abdel-Kader NM, Abdelhady MM, Maged M, Allam AL, Fahmy, SA. Facile sonochemically-assisted bioengineering of titanium dioxide nanoparticles and deciphering their potential in treating breast and lung cancers: biological, molecular, and computational-based investigations. RSC Adv. 2024;14(12):8583–8601.
[8] El-Hawary SS, El-Hefnawy HM, Osman SM, Mostafa ES, Mokhtar FA, El-Raey MA. Chemical profile of two Jasminum Sambac L.(Ait) cultivars cultivated in Egypt-their mediated silver nanoparticles synthesis and selective cytotoxicity. 2019.
[9] Alotaibi B, Negm WA, Elekhnawy E, et al. Antibacterial activity of nano zinc oxide green-synthesised from *Gardenia thailandica* triveng. Leaves against *Pseudomonas aeruginosa* clinical isolates: *in vitro* and *in vivo* study. Artif Cells Nanomed Biotechnol. 2022;50(1):96–106. doi: 10.1080/21691401.2022.2056191.
[10] Wang C, Lin X, Zhang X, et al. Research advances on production and application of algal biochar in environmental remediation. Environ Pollut. 2024;348:123860. doi: 10.1016/j.envpol.2024.123860.
[11] Khanna K, Sharma N, Ohri P, Bhardwaj R. Emerging trends of nanoparticles in sustainable agriculture: current and future perspectives. Plant Nanopart. 2022;(14):1–52.
[12] Mokhtar FA, Selim NM, Elhawary SS, et al. Green biosynthesis of silver nanoparticles using *Annona glabra* and *Annona squamosa* extracts with antimicrobial, anticancer, apoptosis potentials, assisted by in silico modeling, and metabolic profiling. Pharmaceuticals. 2022;15(11):1354. doi: 10.3390/ph15111354.
[13] Roy M, Roy A, Rustagi S, et al. An overview of nanomaterial applications in pharmacology. Biomed Res Int. 2023;2023(1):4838043. doi: 10.1155/2023/4838043.
[14] Idris DS, Roy A. Antioxidant and dye degradation activity of green synthesized silver-iron oxide (Ag-Fe_2O_3) bimetallic nanoparticles. Nano Struct Nano-Objects. 2024;38:101142. doi: 10.1016/j.nanoso.2024.101142.
[15] Gupta A, Haque B, Roy A, et al. Antioxidant, dye degradation, and molecular docking studies of orange peel extract derived Ag-Fe-Ni nanoparticles. Inorg Chem Commun. 2024;166:112599. doi: 10.1016/j.inoche.2024.112599.
[16] Vohra K, Gupta VK. Pharmacognostic evaluation of *Lens culinaris* Medikus seeds. Asian Pacific J Trop Biomed. 2012;2(3):S1221–S1226. doi: 10.1016/S2221-1691(12)60389-X.
[17] Migliozzi M, Thavarajah D, Thavarajah P, et al. Lentil and kale: complementary nutrient-rich whole food sources to combat micronutrient and calorie malnutrition. Nutrients. 2015;7(11):9285–9298. doi: 10.3390/nu7115471.
[18] Hoover R, Hughes T, Chung HJ, et al. Composition, molecular structure, properties, and modification of pulse starches: a review. Food Res Int. 2010;43(2):399–413. doi: 10.1016/j.foodres.2009.09.001.
[19] Ryan E, Galvin K, O'Connor TP, et al. Phytosterol, squalene, tocopherol content and fatty acid profile of selected seeds, grains, and legumes. Plant Foods Hum Nutr. 2007;62(3):85–91. doi: 10.1007/s11130-007-0046-8.
[20] Thavarajah D, Thavarajah P, Sarker A, et al. A global survey of effects of genotype and environment on selenium concentration in lentils (*Lens culinaris* L.): implications for nutritional fortification strategies. Food Chem. 2011;125(1):72–76. doi: 10.1016/j.foodchem.2010.08.038.
[21] Oduro-Yeboah C, Sulaiman R, Uebersax MA, et al. A review of lentil (*Lens culinaris* Medik) value chain: postharvest handling, processing, and processed products. Legume Sci. 2023;5(2):e171. doi: 10.1002/leg3.171.
[22] Amarowicz R, Estrella I, Hernández T, et al. Antioxidant activity of a red lentil extract and its fractions. Int J Mol Sci. 2009;10(12):5513–5527. doi: 10.3390/ijms10125513.
[23] Amarowicz R, Estrella I, Hernández T, et al. Free radical-scavenging capacity, antioxidant activity, and phenolic composition of green

lentil (*Lens culinaris*). Food Chem. 2010;121(3):705–711. doi: 10.1016/j.foodchem.2010.01.009.
[24] Xu B, Yuan S, Chang S. Comparative analyses of phenolic composition, antioxidant capacity, and color of cool season legumes and other selected food legumes. J Food Sci. 2007;72(2):S167–S177. doi: 10.1111/j.1750-3841.2006.00261.x.
[25] Kalogeropoulos N, Chiou A, Ioannou M, et al. Nutritional evaluation and bioactive microconstituents (phytosterols, tocopherols, polyphenols, triterpenic acids) in cooked dry legumes usually consumed in the Mediterranean countries. Food Chem. 2010;121(3):682–690. doi: 10.1016/j.foodchem.2010.01.005.
[26] Güçlü-Ustündağ O, Mazza G. Saponins: properties, applications and processing. Crit Rev Food Sci Nutr. 2007;47(3):231–258. doi: 10.1080/10408390600698197.
[27] Stephen AM, Dahl WJ, Sieber GM, et al. Effect of green lentils on colonic function, nitrogen balance, and serum lipids in healthy human subjects. Am J Clin Nutr. 1995;62(6):1261–1267. doi: 10.1093/ajcn/62.6.1261.
[28] Shi L, Arntfield SD, Nickerson M. Changes in levels of phytic acid, lectins and oxalates during soaking and cooking of Canadian pulses. Food Res Int. 2018;107:660–668. doi: 10.1016/j.foodres.2018.02.056.
[29] Giday M, Teklehaymanot T, Animut A, et al. Medicinal plants of the Shinasha, Agew-awi and Amhara peoples in northwest Ethiopia. J Ethnopharmacol. 2007;110(3):516–525. doi: 10.1016/j.jep.2006.10.011.
[30] Teklehaymanot T, Giday M, Medhin G, et al. Knowledge and use of medicinal plants by people around Debre Libanos monastery in Ethiopia. J Ethnopharmacol. 2007;111(2):271–283. doi: 10.1016/j.jep.2006.11.019.
[31] Sezik E, Yeşilada E, Honda G, et al. Traditional medicine in Turkey X. Folk medicine in central Anatolia. J Ethnopharmacol. 2001;75(2–3):95–115. doi: 10.1016/s0378-8741(00)00399-8.
[32] Ganesan K, Xu B. Polyphenol-rich lentils and their health promoting effects. Int J Mol Sci. 2017;18(11):2390. doi: 10.3390/ijms18112390.
[33] Adebamowo CA, Cho E, Sampson L, et al. Dietary flavonols and flavonol-rich foods intake and the risk of breast cancer. Int J Cancer. 2005;114(4):628–633. doi: 10.1002/ijc.20741.
[34] Jain MG, Hislop GT, Howe GR, et al. Plant foods, antioxidants, and prostate cancer risk: findings from case-control studies in Canada. Nutr Cancer. 1999;34(2):173–184. doi: 10.1207/S15327914NC3402_8.
[35] Agurs-Collins T, Smoot D, Afful J, et al. Legume intake and reduced colorectal adenoma risk in African-Americans. J Natl Black Nurses Assoc. 2006;17(2):6–12.
[36] Nichenametla SN, Taruscio TG, Barney DL, et al. A review of the effects and mechanisms of polyphenolics in cancer. Crit Rev Food Sci Nutr. 2006;46(2):161–183. doi: 10.1080/10408390591000541.
[37] Roy F, Boye J, Simpson B. Bioactive proteins and peptides in pulse crops: pea, chickpea and lentil. Food Res Int. 2010;43(2):432–442. doi: 10.1016/j.foodres.2009.09.002.
[38] Chen C, Kong A-NT. Dietary cancer-chemopreventive compounds: from signaling and gene expression to pharmacological effects. Trends Pharmacol Sci. 2005;26(6):318–326. doi: 10.1016/j.tips.2005.04.004.
[39] Arthur JR, McKenzie RC, Beckett GJ. Selenium in the immune system. J Nutr. 2003;133(5 Suppl 1):1457S–1459S. doi: 10.1093/jn/133.5.1457S.
[40] Bruce WR, Giacca A, Medline A. Possible mechanisms relating diet and risk of colon cancer. Cancer Epidemiol Prevent Biomark. 2000;9(12):1271–1279.
[41] Mo'ez Al-Islam EF, Mohammad MG, Soliman S. Lentils (*Lens culinaris* L.): a candidate chemopreventive and antitumor functional food. Funct Foods Cancer Prevent Ther. 2020;:99–120.
[42] Vohra K, Garg V, Dureja H. Ethnopharmacology, phytochemistry and pharmacology of *Lens culinaris* Medikus seeds: an update. CNF. 2019;15(2):121–129. doi: 10.2174/1573401313666170925155508.
[43] Shams S, Pourseyedi S, Raisi M. Green synthesis of Ag nanoparticles in the present of *Lens culinaris* seed exudates. Int J Agricult Crop Sci. 2013;5(23):2812–2815.
[44] Mohammed HA, Khan RA, Abdel-Hafez AA, et al. Phytochemical profiling, *in vitro* and *in silico* anti-microbial and anti-cancer activity evaluations and *Staph GyraseB* and h-TOP-IIβ receptor-docking studies of major constituents of *Zygophyllum coccineum* L. Aqueous-ethanolic extract and its subsequent fractions: an approach to validate traditional phytomedicinal knowledge. Molecules. 2021;26(3):577. doi: 10.3390/molecules26030577.
[45] Tsugawa H, Cajka T, Kind T, et al. MS-DIAL: data-independent MS/MS deconvolution for comprehensive metabolome analysis. Nat Methods. 2015;12(6):523–526. doi: 10.1038/nmeth.3393.
[46] Albalawi MA, Hafez AM, Elhawary SS, et al. The medicinal activity of lyophilized aqueous seed extract of *Lepidium sativum* L. in an androgenic alopecia model. Sci Rep. 2023;13(1):7676. doi: 10.1038/s41598-023-33988-1.
[47] ELhabal SF, Elwy HM, Hassanin S, et al. Biosynthesis and characterization of gold and copper nanoparticles from *Salvadora persica* fruit extracts and their biological properties. Int J Nanomedicine. 2022;17:6095–6112. doi: 10.2147/IJN.S385543.
[48] Azzazy HM, Sawy AM, Abdelnaser A, Meselhy MR, Shoeib T, Fahmy SA. Peganum harmala alkaloids and tannic acid encapsulated in PAMAM dendrimers: improved anticancer activities as compared to doxorubicin. ACS Appl Poly Mat. 2022;4(10):7228–7239.
[49] Attallah NGM, Elekhnawy E, Negm WA, et al. *In vivo* and *in vitro* antimicrobial activity of biogenic silver nanoparticles against *Staphylococcus aureus* clinical isolates. Pharmaceuticals. 2022;15(2):194. doi: 10.3390/ph15020194.
[50] Aboomar NM, Essam O, Hassan A, et al. Exploring a repurposed candidate with dual hIDO1/hTDO2 inhibitory potential for anticancer efficacy identified through pharmacophore-based virtual screening and *in vitro* evaluation. Sci Rep. 2024;14(1):9386. doi: 10.1038/s41598-024-59353-4.
[51] Hou L, Shi Y, Zhai P, et al. Antibacterial activity and *in vitro* anti-tumor activity of the extract of the larvae of the housefly (*Musca domestica*). J Ethnopharmacol. 2007;111(2):227–231. doi: 10.1016/j.jep.2006.11.015.
[52] Clinical and Laboratory Standards Institute. Performance standards for antimicrobial susceptibility testing, M100. 30th edition. Clinical and Laboratory Standards Institute; 2020.
[53] An W, Lai H, Zhang Y, et al. apoptotic pathway as the therapeutic target for anticancer traditional Chinese medicines. Front Pharmacol. 2019;10:758. doi: 10.3389/fphar.2019.00758.
[54] Ball HS, Girma MB, Zainab M, et al. Characterization and inhibition of 1-Deoxy-d-xylulose 5-phosphate reductoisomerase: a promising drug target in *Acinetobacter baumannii* and *Klebsiella pneumoniae*. ACS Infect Dis. 2021;7(11):2987–2998. doi: 10.1021/acsinfecdis.1c00132.
[55] Morris GM, Goodsell DS, Huey R, et al. Distributed automated docking of flexible ligands to proteins: parallel applications of AutoDock 2.4. J Comput Aided Mol Des. 1996;10(4):293–304. doi: 10.1007/BF00124499.
[56] Ross BJ. A Lamarckian evolution strategy for genetic algorithms. In: Practical handbook of genetic algorithms. CRC Press; 2019. p. 1–16.
[57] Biovia DS. Discovery studio visualizer v21. 1.0. 20298. San Diego: Dassault Systèmes; 2021.
[58] Chang C-S, Yeh TS. Detection of 10 sweeteners in various foods by liquid chromatography/tandem mass spectrometry. J Food Drug Anal. 2014;22(3):318–328. doi: 10.1016/j.jfda.2014.01.024.
[59] Mena P, Calani L, Dall'Asta C, et al. Rapid and comprehensive evaluation of (poly) phenolic compounds in pomegranate (*Punica granatum* L.) juice by UHPLC-MSn. Molecules. 2012;17(12):14821–14840. doi: 10.3390/molecules171214821.
[60] Mekky RH, Contreras MdM, El-Gindi MR, et al. Profiling of phenolic and other compounds from Egyptian cultivars of chickpea (*Cicer arietinum* L.) and antioxidant activity: a comparative study. RSC Adv. 2015;5(23):17751–17767. doi: 10.1039/C4RA13155J.
[61] March RE, Miao XS, Metcalfe CD. A fragmentation study of a flavone triglycoside, kaempferol-3-O-robinoside-7-O-rhamnoside. Rapid Commun Mass Spectrom. 2004;18(9):931–934. doi: 10.1002/rcm.1428.

[62] Li Y, Guang C, Zhao N, et al. LC–MS/MS method for simultaneous determination of linarin and its metabolites in rat plasma and liver tissue samples: application to pharmacokinetic and liver tissue distribution study after oral administration of linarin. Molecules. 2019;24(18):3342. doi: 10.3390/molecules24183342.

[63] Singh C, Upadhyay R, Tiwari KN. Comparative analysis of the seasonal influence on polyphenolic content, antioxidant capacity, identification of bioactive constituents and hepatoprotective biomarkers by *in silico* docking analysis in *Premna integrifolia* L. Physiol Mol Biol Plants. 2022;28(1):223–249. doi: 10.1007/s12298-021-01120-0.

[64] Ersoy E, Eroglu Ozkan E, Boga M, et al. Anti-aging potential and anti-tyrosinase activity of three Hypericum species with focus on phytochemical composition by LC–MS/MS. Ind Crops Prod. 2019;141:111735. doi: 10.1016/j.indcrop.2019.111735.

[65] Cechinel-Zanchett CC, Bolda Mariano LN, Boeing T, et al. Diuretic and renal protective effect of kaempferol 3-O-alpha-l-rhamnoside (afzelin) in normotensive and hypertensive rats. J Nat Prod. 2020;83(6):1980–1989. doi: 10.1021/acs.jnatprod.0c00274.

[66] Venkatalakshmi P, Vadivel V, Brindha P. Identification of flavonoids in different parts of *Terminalia catappa* L. Using LC-ESI-MS/MS and investigation of their anticancer effect in EAC cell line model. J Pharmaceut Sci Res. 2016;8(4):176.

[67] Zhao H-Y, Fan M-X, Wu X, et al. Chemical profiling of the Chinese herb formula Xiao-Cheng-Qi decoction using liquid chromatography coupled with electrospray ionization mass spectrometry. J Chromatogr Sci. 2013;51(3):273–285. doi: 10.1093/chromsci/bms138.

[68] Bystrom LM, Lewis BA, Brown DL, et al. Characterisation of phenolics by LC–UV/Vis, LC–MS/MS and sugars by GC in *Melicoccus bijugatus* Jacq.'Montgomery'fruits. Food Chem. 2008;111(4):1017–1024. doi: 10.1016/j.foodchem.2008.04.058.

[69] Lin L-Z, Harnly JM. Identification of the phenolic components of chrysanthemum flower (*Chrysanthemum morifolium* Ramat). Food Chem. 2010;120(1):319–326. doi: 10.1016/j.foodchem.2009.09.083.

[70] Davarcı A, Kadiroğlu P, Dıblan S, et al. Influence of processing steps on phenolic composition of clarified and unclarified pomegranate juices as characterized by LC-DAD-ESI-MS/MS. J Food Process Preserv. 2019;43(8):e14018. doi: 10.1111/jfpp.14018.

[71] Abdel-Hamed AR, Mehanna ET, Hazem RM, et al. Plicosepalus acacia extract and its major constituents, methyl gallate and quercetin, potentiate therapeutic angiogenesis in diabetic hind limb ischemia: HPTLC quantification and LC-MS/MS metabolic profiling. Antioxidants. 2021;10(11):1701. doi: 10.3390/antiox10111701.

[72] Routaboul J-M, Kerhoas L, Debeaujon I, et al. Flavonoid diversity and biosynthesis in seed of *Arabidopsis thaliana*. Planta. 2006;224(1):96–107. doi: 10.1007/s00425-005-0197-5.

[73] Li A, Hou X, Wei Y. Fast screening of flavonoids from switchgrass and *Mikania micrantha* by liquid chromatography hybrid-ion trap time-of-flight mass spectrometry. Anal Methods. 2018;10(1):109–122. doi: 10.1039/C7AY02103H.

[74] Li Y-y, Song Y-y, Liu C-h, et al. Simultaneous determination of esculin and its metabolite esculetin in rat plasma by LC–ESI-MS/MS and its application in pharmacokinetic study. J Chromatogr B Analyt Technol Biomed Life Sci. 2012;907:27–33. doi: 10.1016/j.jchromb.2012.08.027.

[75] Binsuwaidan R, Elekhnawy E, Elseady WS, et al. Antibacterial activity and wound healing potential of *Cycas thouarsii* R. Br n-butanol fraction in diabetic rats supported with phytochemical profiling. Biomed Pharmacother. 2022;155:113763. doi: 10.1016/j.biopha.2022.113763.

[76] Río J, Fuster MD, Sabater F, et al. Selection of citrus varieties highly productive for the neohesperidin dihydrochalcone precursor. Food Chem. 1997;59(3):433–437. doi: 10.1016/S0308-8146(96)00303-2.

[77] She G, Wang S, Liu B. Dihydrochalcone glycosides from *Oxytropis myriophylla*. Chem Cent J. 2011;5(1):71. doi: 10.1186/1752-153X-5-71.

[78] Kiran S, et al. Commercial lentils (*Lens culinaris*) provide antioxidative and broad-spectrum anti-cancerous effects. Legume Res. 2021;44(2):202–206.

[79] Chan YS, Yu H, Xia L, et al. Lectin from green speckled lentil seeds (*Lens culinaris*) triggered apoptosis in nasopharyngeal carcinoma cell lines. Chin Med. 2015;10(1):25. doi: 10.1186/s13020-015-0057-6.

[80] Bin-Jumah M, Al-Abdan M, Albasher G, et al. Effects of green silver nanoparticles on apoptosis and oxidative stress in normal and cancerous human hepatic cells *in vitro*. Int J Nanomedicine. 2020;15:1537–1548. doi: 10.2147/IJN.S239861.

[81] Agrawal SB, Gupta N, Bhagyawant SS, et al. Anticancer activity of lectins from *Bauhinia purpurea* and *Wisteria floribunda* on breast cancer MCF-7 cell lines. Protein Pept Lett. 2020;27(9):870–877. doi: 10.2174/0929866527666200408143614.

[82] Moreno-Celis U, López-Martínez FJ, Cervantes-Jiménez R, et al. Tepary bean (*Phaseolus acutifolius*) lectins induce apoptosis and cell arrest in G0/G1 by P53 (Ser46) phosphorylation in colon cancer cells. Molecules. 2020;25(5):1021. doi: 10.3390/molecules25051021.

[83] Jung YS, Lee SH, Chun SY, et al. *In vitro* and *in vivo* protective effects of lentil (*Lens culinaris*) extract against oxidative stress-induced hepatotoxicity. Molecules. 2021;27(1):59. doi: 10.3390/molecules27010059.